Global modeling of hydrogen using GFDL-AM4.1: sensitivity of soil removal and radiative forcing

Fabien Paulot[a], David Paynter[a], Vaishali Naik[a], Sergey Malyshev[a], Raymond Menzel[b], Larry W. Horowitz[a]

[a] *Geophysical Fluid Dynamics Laboratory, National Oceanic and Atmospheric Administration, Princeton, New Jersey, USA*
[b] *University Corporation for Atmospheric Research/GFDL, Princeton, New Jersey*

Abstract

Hydrogen (H_2) has been proposed as an alternative energy carrier to reduce the carbon footprint and associated radiative forcing of the current energy system. Here, we describe the representation of H_2 in the GFDL-AM4.1 model including updated emission inventories and improved representation of H_2 soil removal, the dominant sink of H_2. The model best captures the overall distribution of surface H_2, including regional contrasts between climate zones, when $v_d(H_2)$ is modulated by soil moisture, temperature, and soil carbon content. We estimate that the soil removal of H_2 increases with warming (2 to 4% per K), with large uncertainties stemming from different regional response of soil moisture and soil carbon. We estimate that H_2 causes an indirect radiative forcing of 0.84 $\mathrm{mW\,m^{-2}/(Tg(H_2)yr^{-1})}$ or 0.13 $\mathrm{mW\,m^{-2}\,ppbv^{-1}}$, primarily due to increasing CH_4 lifetime and stratospheric water vapor production.

Keywords: Dry deposition, Radiative forcing, Climate change

1. Introduction

H_2 is being investigated as an energy carrier for applications ranging from transportation to industry, heating, and energy storage [1, 2, 3, 4, 5]. Interest for H_2 is partly motivated by the reduction in greenhouse gases that the displacement of fossil fuels by H_2 in such applications may afford. For instance, CO_2-free H_2 (*green hydrogen*) can be produced from water electrolysis if powered by renewable energy sources [6, 7, 8, 9, 10]. Geological storage of *green hydrogen* has been proposed as an avenue to compensate for

the unpredictabilty and intermittency of solar and wind-generated electricity [11, 12, 13, 14]. Reduction in the carbon footprint of the H_2 produced from fossil fuels (*grey hydrogen*), which accounts for 95% of present-day H_2 production [6, 15], may also be achieved via carbon capture and storage (*blue hydrogen*, [16]).

Previous studies have shown that a shift to a *hydrogen economy* would result in improvements in air quality due to reductions in NO_x and CO emissions [17, 18, 19, 20]. The impact of higher anthropogenic H_2 emissions on the Earth's radiative budget is less well understood. While H_2 is not radiatively active, its oxidation tends to increase methane and tropospheric O_3, two potent greenhouse gases [21, 17, 22, 18, 23]. It also increases stratospheric water, which is accompanied by stratospheric cooling [18, 24, 25, 26, 21]. To our knowledge, the indirect radiative forcing associated with H_2 has only been quantified using the STOCHEM model [21, 22, 23] with an estimated H_2 greenhouse warming potential over a 100-year time horizon of 5 ± 1 excluding the impact of H_2 on the stratosphere. Considering the prospects for increasing H_2 usage, it it is important to assess the gaps in our understanding of the present-day H_2 budget and their implications for the sensitivity of H_2 to climate change and the indirect radiative forcing of H_2.

Hydrogen (H_2) is the second most abundant reactive trace gas in the atmosphere with a present day global mean concentration of $\simeq$530 ppbv [27]. H_2 sources include both direct emissions ($\simeq$35 Tg/yr circa 2000, 30% of which from fossil fuel combustion), and formaldehyde photolysis ($\simeq$41 Tg/yr, 55% of associated with methane) [28]. Atmospheric H_2 concentrations exhibit an hemispheric asymmetry with concentrations in the Northern high latitudes $\simeq$ 40 ppbv lower than at the same latitudes in the Southern Hemisphere [28]. This unique pattern has been attributed to the soil removal of H_2, which is estimated to account for over 80% of H_2 removal [27, 28, 29].

H_2 soil removal is thought to be modulated by both the soil diffusivity of H_2 and the activity of hydrogen-oxidizing bacteria. H_2 soil diffusivity (D_s) is well understood [28]. D_s increases with soil temperature but decreases with soil moisture due to the low solubility of H_2. This dependency is broadly consistent with the observed sensitivity of soil H_2 removal in field and laboratory experiments [29, 30, 31, 32, 33, 34, 35, 36].

In contrast, the factors controlling the biological sink are less well understood. Recent studies have demonstrated that the soil removal of H_2 is dominated by high-affinity hydrogen-oxidizing bacteria (HA-HOB, [37, 38]). This class of microorganisms differs from low-affinity H_2-oxidizing bacteria

(LA-HOB), which are found near point sources of H_2 (e.g., legumes, H_2 seepage from underground reservoirs [39, 40]) and are unable to grow using the much lower concentrations of H_2 found in the atmosphere [37, 41]. Many different HA-HOB have recently been identified [42, 43, 44, 45, 46] and considerable progress has been made in characterizing their metabolism [47, 41, 48]. However, large uncertainties remain regarding the activity and spatial distribution of HA-HOB [49].

In this work, we describe and evaluate the representation of H_2 in the GFDL-AM4.1 global chemistry-climate model focusing on the representation of the soil sink. We then characterize the simulated response of H_2 soil removal to global warming and the indirect equilibrium radiative forcing of H_2.

2. Method

We use the GFDL AM4.1 model, the atmospheric component of the Earth System Model 4.1 [50, 51, 52]. The model horizontal resolution is $\simeq$100 km with 49 vertical levels. The model is run with prescribed sea surface temperature and sea ice concentration based on reanalysis [53, 54] (AMIP experiment).

2.1. H_2 *sources*

Sources of H_2 include direct emissions and photochemical production from the photolysis of formadelhyde [28]. H_2 is emitted from biomass burning, fossil fuel combustion, and nitrogen fixation [28]. Biomass burning emissions are estimated using dry matter burnt from BB4MIP [55] with emissions factors from Andreae [56] and Akagi et al. [57] (Table S1). We estimate anthropogenic H_2 emissions from CO emissions taken from the Community Emissions Data System v2017-05-18 [58] using source specific emission factors (Table S2, [28, 59]). The relationship between CO and H_2 emissions reflect the water–gas shift reaction [60]

$$CO_2 + H_2 \qquad CO + H_2O \tag{1}$$

H_2 emissions associated with terrestrial and marine N fixation are set to 3 and 6 Tg/yr [28] and distributed using the soil and oceanic CO emissions, respectively.

Total emissions of H_2 over the 1995–2014 period are 32.3 Tg/yr, which falls within the range of previous estimates (Table 1). However, there are

large differences for individual sources. In particular, while our global source is 8% lower than the estimate of Ehhalt and Rohrer [28], our estimate is 30% higher for anthropogenic emissions and 40% lower for biomass burning. This highlights the significant uncertainties in the magnitude of individual sources of H_2 to the atmosphere.

Fig. 1 shows the estimated H_2 emissions over the 1850–2014 period. Total sources have increased by over 50% from preindustrial to present-day. Emissions peaked in 1997 (37.1 Tg/yr) due to large biomass burning emissions associated with a strong El-Niño. From 1995 to 2014, H_2 emissions have decreased, which is primarily driven by a 40% decrease in transportation emissions.

AM4.1 includes both emission and photochemical production of formaldehyde. Emissions from anthropogenic sources and biomass burning are from CEDS v2017-05-18 (2.4 Tg/yr over the 1995–2014 period) and BB4MIP (4.9 Tg/yr), respectively. We do not consider sources of formaldehyde from vegetation ($\simeq$ 25 Tg/yr [61]). AM4.1 also includes a comprehensive chemical mechanism [52] which accounts for sources of formaldehyde associated with methane and non-methane volatile organic compounds (NMVOCs) oxidation. Global mean surface concentration of CH_4 is prescribed as lower boundary conditions for chemistry. Excluding formaldehyde, AM4.1 includes emissions of 10 NMVOCs (ethane, propane, a lunmped higher-alkane tracer, ethene, propene, isoprene, monoterpenes, methanol, ethanol, and acetone) from anthropogenic sources (CEDS v2017-05-18), biomass burning (BB4MIP) and natural sources (Precursors of Ozone and their Effects in the Troposphere [62]) except for isoprene and monoterpene whose emissions are calculated interactively in the model using the Model of Emissions of Gases and Aerosols from Nature (MEGAN v2.1 [63]). The contribution of directly emitted formaldehyde is much smaller than photochemical production from methane and NMVOCs ($\simeq$ 1670 Tg/yr).

The photolysis of formaldehyde is calculated using FAST-JX [64]. Chemical production over the 1995–2014 period is 42.1 Tg/yr or 56% of the overall H_2 source, in good agreement with previous bottom-up estimates (Table 1). Tropospheric H_2 chemical production increases by 9% (3.6 Tg/yr) over the 1990–2014 period.

2.2. H_2 *sinks*

Sinks of H_2 include atmospheric oxidation and dry deposition. AM4.1 includes oxidation of H_2 by OH (k=$2.8 \times 10^{-12} \exp(-1800/T)$ cm^3/molec/s)

and O^1D ($k = 1.2 \times 10^{-10}$ cm^3/molec/s) following Sander et al. [65]. We use a two layer model to represent H_2 soil removal [31, 66]. In the first layer, H_2 diffuses through an inactive layer which comprises both snow (δ_{snow}) and dry top soil (δ). In the second layer, H_2 is removed by HA-HOB at a rate k_s. Assuming that H_2 is at steady state in the soil, the surface removal of H_2 can be expressed following Ehhalt and Rohrer [66] as:

$$v_d(\mathrm{H_2}) = \frac{1}{\frac{\delta}{D_s} + \frac{\delta_{\text{snow}}}{D_{\text{snow}}} + \frac{1}{\sqrt{D_s k_s \Theta_a}}} \tag{2}$$

This parameterization will be referred to as Ehhalt, hereafter. The soil diffusivity of H_2 (D_s) is calculated following Millington and Quirk [67].

$$D_s = D_a \cdot \frac{\Theta_a^{3.1}}{\Theta_p^2} \tag{3}$$

where Θ_p, Θ_a and D_a are the soil porosity, the soil air fraction (cm^3 air filled pores/cm^3 soil) and the diffusivity of H_2 in air [31] averaged over the first 10 cm, respectively. Snow diffusivity (D_{snow}) is set to 0.64 D_a, using the average of fresh and aged snow diffusivity [68]. δ decreases with soil moisture following Ehhalt and Rohrer [66]. $k_s\Theta_a$ is expressed as:

$$k_s\Theta_a = Af(\Theta_a)g(T_s) \tag{4}$$

where the dependence of k_s on soil moisture ($f(\Theta_a)$) and soil temperature ($g(T_s)$) are calculated following Ehhalt and Rohrer [66]. A reflects the abundance and activity of HA-HOB. A is adjusted such that the average land deposition velocity is 0.035 cm/s over the 1989-2014 period. As we will show in section 3.2, this value provides a reasonable fit to surface H_2 observations. We assume that H_2 surface removal is solely controlled by its soil removal, i.e, we neglect the aerodynamic and laminar resistances, which are both much smaller than the soil resistance [69]. Our global estimate is similar to Yashiro et al. [70] at $v_d = 0.033$ cm/s but much slower than Sanderson et al. [71] (0.053 cm/s). Note that the dependence of v_d on soil moisture is non-monotonic, which is consistent with parameterizations used to represent the microbial removal of gases such as carbon monoxide, methane, and carbonyl sulfide [72, 73, 74]. This differes from previous global studies [75, 70], which assumed no dependence of $k_s\Theta_a$ when the fraction of soil pores filled with water exceeds 15% following Smith Downey [76]. As in previous work,

the Ehhalt parameterization assumes that a mimimum level of soil water is required to activate HA-HOB. The magnitude of this threshold is uncertain, with estimates ranging from 2 to 8% [75, 76, 66].

Dry deposition is the most important sink of H_2 in AM4.1, accounting for over 70% of the tropospheric removal of H_2. This is in good agreement with previous bottom-up estimates but lower than top-down estimates (80%). Yashiro et al. [70] attributed this discrepancy to biases in the top-down estimates due to the limited spatial coverage of measurements and oversimplification of the H_2 budget.

3. Evaluation

3.1. Dry deposition velocity

We use the monthly land properties simulated by LM4.1 (Shevliakova et al., 2020), the land component of the GFDL Earth System Model 4.1 (ESM4.1) averaged over the top 10 cm in the AMIP simulation as inputs to calculate $v_d(H_2)$. Fig. 2 shows the spatial pattern of H_2 deposition velocity simulated using equation (2). $v_d(H_2)$ is maximum in North Africa and the Arabian Peninsula. In these regions, soil moisture is low, which results in high H_2 soil diffusivity, but remains high enough to exceed the threshold for microbial activity. $v_d(H_2)$ is minimum at high latitudes, where low temperature and snow cover tend to inhibit the soil removal of H_2. Soil removal is also low in tropical rain forests as high soil moisture tends to reduce both H_2 soil diffusivity and microbial consumption.

Comparison with field observations (Fig. 3) shows that the model captures the seasonality and magnitude of $v_d(H_2)$ well at Harvard Forest (a), Gif-sur-Yvette (b), and Helsinki (d). However, it underestimates $v_d(H_2)$ at Tsukuba (c), Mace-Head (e), and Heidelberg (g). At all these sites, the simulated H_2 removal is strongly inhibited by high soil moisture. In contrast, the model tends to overestimate $v_d(H_2)$ at the California desert site in summer, when soil moisture is lowest (f) .

Model biases at sites (c) and (e-g) are consistent with a high bias in the soil moisture, used to estimate $v_d(H_2)$. Such bias may be associated with temporal or spatial heterogeneities in soil moisture that are not captured in the LM4.1 monthly model output. Reducing the volumetric soil water content by 0.06 uniformly significantly improves the model performance by increasing removal in temperate and tropical regions (higher soil H_2 diffusivity) and reducing summer time deposition in deserts. Globally, the largest

difference is found in deserts, where the reduction in soil moisture results in more frequent inhibition of H_2 consumption by HA-HOB (Fig. 2). A similar correction was applied by Yashiro et al. [70], who applied a uniform correction of 0.22 to volumetric soil water content in the CHASER model to obtain a reasonable simulation of H_2. This parameterization will be referred to as Ehhalt_M.

Another possible source of bias is the geographical distribution and activity of HA-HOB. Here we assume that HA-HOB are distributed homogeneously, i.e., we do not modulate HA-HOB abundance by microbial biomass, an output of the LM4.1 model. This reflects recent studies that found that a) HA-HOB account for a very small portion of microbial biomass (<1% [49]) and b) HA-HOB are present in environments where nutrients are limiting [77, 78, 47]. Clearly, more research is needed to understand the spatial distribution of HA-HOB.

As described earlier, the activity of HA-HOB is modulated by soil water content and soil temperature. Recent studies [49] also show that HA-HOB activity scales like organic soil carbon content. In order to quantify the impact of such modulation, we assume that A depends on $soilC$ following a Michaelis-Menten relationship ($A = \alpha \frac{\mathrm{soilC}}{\beta + \mathrm{soilC}}$). We select a high $\beta = 7\mathrm{kgC/m^3}$, such that $v_d(H_2)$ dependence in soilC is linear in most environments consistent with observations [49]. α is adjusted to yield the same deposition velocity as the Ehhalt parameterization over the 1989–2014 period. This parameterization will be referred to as Ehhalt_MC. Fig. 2 shows that modulation by $soilC$ leads to faster deposition in the tropics and high latitudes and slower deposition in arid regions. However, the Ehhalt_M and Ehhalt_MC parameterizations are largely indistinguishable at the mid-latitude locations for which we have extended measurements of $v_d(H_2)$ (Fig. 3)

We also consider the parameterizations of Price [79] and Sanderson [71]. The Price parameterization assumes the same deposition velocity for all soil types. Soil removal is reduced at low temperature ($T < 0°\mathrm{C}$). The Sanderson parameterization uses ecosystem-specific deposition velocities based on field observations. A dependence of H_2 on soil moisture is considered for certain ecosystems (agriculture, savannah, forest, grassland) but no dependence on temperature. Both the Price and Sanderson parameterizations account for the inhibition of soil H_2 removal in the presence of snow. To facilitate comparisons, we scale the simulated annual global deposition velocity from both

schemes to yield the same value as the Ehhalt_M parameterization over the 1989–2014 period.

Fig. 3 shows that the Price scheme captures best the small spread in maximum $v_d(H_2)$ across sites but underestimates the seasonality of $v_d(H_2)$. It is the only parameterization that captures the elevated $v_d(H_2)$ at Mace Head and Tsukuba (Fig 3c and e), where both the Ehhalt and Sanderson parameterizations exhibit too much inhibition by high soil moisture. The performance of the Sanderson scheme is largely consistent with that of the Ehhalt-based parameterizations. The Sanderson scheme tends to underestimate the seasonality of $v_d(H_2)$ at Harvard forest (a) and Helsinki (d), which may reflect the lack of temperature dependence. The complete inhibition of H_2 deposition in deserts in the Sanderson scheme is not supported by observations collected by Smith-Downey et al. [33] (shown in Fig. 3f) and Conrad and Seiler [29].

Fig. 2 shows that the largest regional differences between the different parameterizations of $v_d(H_2)$ are found in the subtropics, where the Ehhalt_MC and Sanderson schemes show depressed removal, consistent with previous simulations by Morfopoulos et al. [75] and in tropical regions, where high moisture reduces H_2 soil removal in the Ehhalt and Ehhalt_M scheme. In contrast, Yashiro et al. [70] simulations suggest that the fastest soil removal for H_2 occurs in tropical regions. The increase in $v_d(H_2)$ in tropical regions in Ehhalt_M relative to Ehhalt suggests that differences between the spatial distribution of $v_d(H_2)$ across models can be largely ascribed to differences in soil moisture and its impact on HA-HOB activity. As we will discuss in Section 4.1, uncertainties regarding the relative deposition velocity of H_2 in tropical and subtropical environments have important implications for the sensitivity of H_2 removal to global warming.

3.2. Surface concentration

Fig. 4 shows the seasonal distribution of surface atmospheric H_2 concentrations in AM4.1. Here, we prescribe monthly $v_d(H_2)$ using the Ehhalt_MC parameterization as described in section 3.1. Observations from NOAA Global Monitoring Laboratory [27], the Advanced Global Atmospheric Gases Experiment (AGAGE [80]) and the Commonwealth Scientific and Industrial Research Organisation (CSIRO [81]) are shown as colored diamonds. CSIRO and AGAGE observation use the Max Plank Institute calibration [82], while NOAA observations follow Novelli et al. [27]. The NOAA calibration is less stable, which may introduce biases [82]. At the Cape Grim, Alert, and

South Pole stations, we find that H_2 from NOAA is on average 1.9% lower than CSIRO observations and we apply this correction factor for all NOAA observations.

Observations indicate that H_2 surface concentrations are lowest in fall in the Northern middle and high latitudes, a pattern that is well captured by the model with seasonal biases and R^2 ranging from 0.5 to 8.3 ppbv and 0.51 to 0.83, respectively (Fig. S1). Because of H_2 long lifetime, the model performance largely reflect the regional distribution of H_2 sources (e.g., high emissions in China) and the degree of isolation of each site from oceanic influence (low concentrations over central Asia) rather than the regional variability in the soil removal of H_2. This is illustrated in Fig. 5, which shows that the Price parameterization captures differences in observed H_2 surface concentrations across climate zones well even though $v_d(H_2)$ is constant outside of the high latitudes. However, the Ehhalt_MC parameterization reduces the model low-bias in hot deserts (BWh), Mediterranean hot summer climate (Csa) and hot semi-arid climates (BSh). This provides additional support for the inhibition of H_2 removal in arid climates. We note that the Ehhalt_M shows much less improvements in these regions (Fig. 5), consistent with the lack of inhibition of microbial activity by soil moisture in these regions (Fig. 2). This results in slightly worse performances overall relative to the Ehhalt_MC parameterization (Fig. S1). Regardless of the parameterization, AM4.1 overestimates the low concentrations of H_2 observed at the KZD (Kazakhstan), UUM (Mongolia), and UTA (Western United States) sites especially in DJF (mean bias $>$ 50 ppbv). More observations are needed to understand the processes that control H_2 removal in these continental and arid regions.

NOAA observations are not available after 2005 because of the aforementioned calibration issues and we have focused our evaluation on the long-term climatology of surface H_2 concentrations. However, we note that the decrease in transportation emissions discussed previously causes a small decrease in H_2 surface concentration at Northern Hemisphere sites over the 2000–2014 period. This decrease is not supported by CSIRO observations at Mace Head and Alert (not shown). Because of the unavailability of NOAA observations (which account for over 80% of the surface sites) after 2005, it is not possible to assess whether this discrepancy is robust. However, we note that several factors could counteract the simulated decline in H_2 emissions, including a) changes in the H_2 emission factor relative to CO due to changes in engines and fuel mix [83, 59] and b) 1–4% leakage [83] of industrial H_2 (primarily for NH_3 and methanol production) for which demand has increased by 60 Tg/yr

from 1990 to 2015.

4. Discussion

4.1. Sensitivity of H_2 *deposition velocity to climate change*

To estimate the sensitivity of the soil removal of H_2 to climate change, we calculate $v_d(H_2)$ using monthly soil properties simulated by ESM4.1 under different forcing scenarios: 1) a 1%/yr increase in CO_2 concentration relative to preindustrial conditions (1pct) and 2) the historical evolution of natural and anthropogenic forcings (Historical) extended up to 2100 using the Shared Socioeconomic Pathways scenario 3-7.0 (SSP3-7.0). The SSP3-7.0 scenario is characterized by high emissions of well-mixed greenhouse gases and short-lived climate forcers as well as substantially high land use by 2100 [84]. The historical and 1pct experiments are part of the DECK (Diagnostic, Evaluation and Characterization of Klima) for the Coupled Model Intercomparison Project phase 6 (CMIP6). The SSP3-7.0 experiment is part of the ScenarioMIP project [85].

Fig. 6 shows the simulated response of $v_d(H_2)$ relative to preindustrial conditions. $v_d(H_2)$ is simulated to increase by 1.9 to 4.3%/K depending on the forcing scenario and v_d parameterization. Using the Ehhalt_M parameterization, the increase in $v_d(H_2)$ is largely insensitive to the forcing scenario (1.9–2.7%/K). This is similar to the responses simulated with the Sanderson (1.6–2.1%/K) and Price (1.4%/K) parameterizations (not shown). Regionally, v_d increases over most of the Northern midlatitudes and in the tropics but decreases in the subtropics (Fig. S5). Changes in the tropics and subtropics are due to dryer soils (Fig. S2). In the tropics, drying tends to increase H_2 removal, both through faster diffusivity and greater HA-HOB activity. In the subtropics, the faster diffusivity is more than compensated by reduced microbial activity, as the minimum soil moisture threshold for microbial activity is less frequently met. In the Northern mid and high latitudes, the increase in $v_d(H_2)$ is dominated by greater HA-HOB activity associated with higher temperature. In some regions (e.g., Central Europe), the increase in soil moisture causes $v_d(H_2)$ to decrease. We note that the response of soil liquid and total water content to warming in ESM4.1 is qualitatively similar to the multi-model median from CMIP6 (Figs S3 and S4), which suggests that the regional trends discussed above are robust. One notable exception is Central Europe, where ESM4.1 shows larger increase in soil moisture

than the CMIP6 median, which would result in stronger inhibition of H_2 soil removal.

The magnitude of the response of $v_d(H_2)$ to warming is more sensitive to the forcing scenario when the Ehhalt_MC parameterization is adopted. In the 1pct experiment, v_d exhibits a stronger response to warming than under the Ehhalt_M parameterization (4.3%/K vs 1.9%/K). This reflects the distribution of soil C, which tends to amplify the increase of $v_d(H_2)$ in the tropics and Northern midlatitudes, while dampening its decrease in the subtropics. However, under the hist_ssp scenario, the sensitivity of $v_d(H_2)$ to warming is reduced by 35% (2.8%/K). The reduced sensitivity reflects the decrease in soil C associated with land-use change in the midlatitudes, which counteracts the increase of $v_d(H_2)$ associated with changes in soil moisture and temperature. This highlights the need to understand how HA-HOB activity may be modulated by anthropogenic activities (e.g., agriculture, irrigation). More broadly, more research is needed to understand how HA-HOB spatial distribution and the sensitivity of HA-HOB activity to environmental parameters (e.g., soil temperature and moisture and labile carbon), both of which are assumed constant here, may also be altered by climate change.

4.2. Indirect radiative effect of H_2

H_2 indirectly modulates Earth's radiative balance. First, H_2 oxidation increases the lifetime of methane, a potent greeenhouse gas, by depleting its primary oxidant, OH. Second, the oxidation of H_2 produces HO_2 radicals, which reacts with NO to produce tropospheric O_3, a pollutant and greenhouse gas. Finally, H_2 oxidation is a source of stratospheric water, which tends to cool the stratosphere, an additional positive forcing.

Here, we use AM4.1 to estimate the Effective Radiative Forcing (ERF) of H_2. In the reference simulation (REF), AM4.1 is run for 50 years with repeating emissions, SST and SIC based on 2010 conditions. Monthly $v_d(H_2)$ is based on the Ehhalt_MC parameterization averaged over the 1995–2010 period. We then perform a perturbation experiment in which H_2 anthropogenic emissions are increased by 200 Tg/yr. This experiment will be referred to as HIGH_H2. To put the magnitude of this perturbation in context, we compare it with different scenarios for future H_2 demand. Derwent et al. [22] estimated that a complete replacement of fossil fuels under present-day conditions would require 2500 Tg/yr of H_2. An additional 200 Tg/yr would thus amount to an 8% leakage rate. This is likely an upper bound with literature estimates ranging from 0.3% to 10% [83, 19]. More realistic scenarios

suggest an increase in anthropogenic H_2 production of up to 550 Tg/yr by 2050 [86, 87, 1]. Assuming a high leakage rate of 10%, such transition to a *hydrogen economy* would result in an increase in anthropogenic H_2 emissions $\simeq 25\%$ that considered here.

We find that the increase in anthropogenic H_2 emissions is accompanied by a 7% decrease in tropospheric OH and an 8% increase in CH_4 lifetime. As CH_4 surface concentration is prescribed in AM4.1, the increase in CH_4 concentration associated with higher H_2 emissions is not accounted for in the HIGH_H2 simulation. Following West et al. [88] and Fiore et al. [89], we estimate the long-term change in CH_4 concentration as

$$[CH_4]_p = [CH_4]_0 \left(\frac{\tau_p}{\tau_0}\right)^F \tag{5}$$

where τ and $[CH_4]$ are the lifetime and concentration of methane, respectively and F is the methane feedback lifetime parameter. We use the subscripts 0 and p to denote the REF and HIGH_H2 experiments, respectively. $F = 1.3$ in AM4.1 [90] with literature estimates ranging from 1.25 to 1.45 [89, 90]. To estimate the overall H_2 ERF, we perform another experiment in which anthropogenic emissions of H_2 are increased by 200 Tg and surface CH_4 is increased from $[CH_4]_0 = 1808$ to $[CH_4]_p = 2005$ ppbv. This experiment will be referred to as HIGH_H2_CH4 hereafter.

H_2 burden is 3.48× greater in HIGH_H2_CH4 relative to the REF simulation, which is 3% less than the increase in H_2 source. This small negative feedback is attributed to the larger response of surface H_2 concentrations (3.58×), which favors soil removal. This change in the vertical distribution of H_2 results in a 3% decrease in H_2 lifetime in spite of decreasing tropospheric OH (-9%).

The simulated response of H_2 burden to increasing H_2 emissions does not consider possible changes in $v_d(H_2)$. To our knowledge, the sensitivity of HA-HOB to small ($< 5\times$) perturbations in H_2 concentrations has not been quantified, with previous studies focusing on much larger perturbations (1000× or more) such as those associated with legumes [40] or seepage of deep H_2 reservoirs [39]. In general, the activity of HA-HOB scales like $[H_2]/([H_2] + K_m)$, where K_m is the half saturation of HA-HOB. If $[H_2] \gg K_m$, the magnitude of the soil sink will not increase in response to higher H_2 emissions and $[H_2]$ concentration would increase more than 10× in the HIGH_H2_CH4 experiment. However, such saturation seems unlikely as reported K_m for HA-HOB are

more than 50× the present-day concentration of H_2 [41]. Higher H_2 emission may also favor HA-HOB growth, which could lead to an increase in $v_d(H_2)$ thus dampening the atmospheric response of atmospheric H_2 to higher anthropogenic emissions. Furthermore, as noted in the previous section, our model suggests $v_d(H_2)$ will increase in future decades as the planet warms. Clearly more laboratory and field experiments are needed to characterize the response of HA-HOB to realistic perturbations in atmospheric H_2 that may arise due to the development of a *hydrogen economy*.

The increase in H_2 emissions results in higher tropospheric O_3 (+1.3 DU and Fig. 7a) and higher stratosphere water (Fig. 7b) (+4.9%). The spatial pattern and magnitude of the increase in stratospheric water vapor is consistent with the results of Warwick et al. [91], who reported an increase of 3.4% for a 2.5× perturbation to surface H_2 concentration. ESM4.1 shows little response in stratospheric O_3 (+0.4%, Fig. 7b). In particular, we find that the increase in H_2 emissions causes little change in polar stratospheric clouds and stratospheric O_3 depletion. This agrees well with previous studies suggesting H_2 is unlikely to cause large changes in stratospheric O_3 [91, 25].

We estimate that an increase in H_2 emissions of 200 Tg/yr causes a positive radiative forcing of +0.17 $\mathrm{W\,m^{-2}}$, based on the change in the radiative imbalance at the top of the atmosphere in the HIGH_H2_CH4 experiment relative to the REF experiment. In order to understand the relative contribution of changes in methane, ozone, and water vapor to H_2 ERF, we perform off-line radiative transfer calculations. We place the global mean perturbation of methane, stratospheric water, stratospheric ozone in to the radiation code that contains an estimate of the global mean atmospheric state and account for stratospheric temperature change using fixed-dynamical heating calculations (FDH) [92]. Following Myhre et al. [93] and Etminan et al. [94] the adjustment due to stratospheric cooling for each forcing scenario is calculated by adding a fixed heating term (equal in magnitude, but opposite in sign to present-day cooling rates) to all points in the stratosphere, and then iterating an offline radiative transfer model (in this case RTE+RRTMGP, see Pincus et al. [95]) until the stratospheric temperature reaches equilibrium. We estimate that methane, tropospheric ozone, stratospheric ozone, and stratospheric water contribute 46%, 21%, 5%, and 28% to H_2 ERF. One third of H_2 ERF is associated with the stratospheric response, mainly due to cooling and increased greenhouse trapping in the lower stratosphere associated with greater water vapor production (from both CH_4 and H_2 oxidation).

Assuming linearity, this suggests an ERF efficiency of 0.84 $\mathrm{mW\,m^{-2}/(Tg\,yr^{-1})}$

or 0.13 mW m^{-2}/ppbv. Recent CMIP6 estimates of the Earth's climate sensitivity, i.e., the long-term increase in temperature induced by a doubling of CO_2 (ERF=3.98 W m^{-2} [96]) range from 2.29K to 5.64K with an average of 3.8K [97, 98]. Assuming that the radiative forcing induced by H_2 has the same efficacy as the radiative forcing from CO_2 [99], we estimate that a sustained 50 Tg/yr increase in the anthropogenic emissions of H_2 (a pessimistic scenario, as discussed earlier) would result in 0.04 K (0.025–0.059K) increase in global surface temperature.

Conclusion

We have described and evaluated the representation of H_2 in the GFDL AM4.1 model. Our simulated global budget is consistent with previous bottom-up inventories with similar contributions of photochemical and surface emissions to the overall source of H_2. Large uncertainties are however noted regarding the magnitude of anthropogenic and biomass burning H_2 emissions. Comparison between different representations of soil H_2 consumption, the dominant removal mechanism for atmospheric H_2, shows considerable differences in the tropics and subtropics, which reflect uncertainties in soil moisture and the sensitivity of HA-HOB activity to soil moisture and soil carbon. This highlights the need for long-term observations of $v_d(H_2)$ and H_2 concentration in tropical forests and arid regions.

We estimate that $v_d(H_2)$ exhibits a positive sensitivity to warming (1.9–4.3%/K). Regionally, dryer soils result in faster removal of H_2 in tropical regions but slower removal in the subtropics. More work is needed to understand how the spatial distribution and activity of HA-HOB may be altered by changes in environmental conditions including increasing H_2 concentration.

We estimate that the H_2 ERF efficiency is 0.84 mW m^{-2}/(Tg yr^{-1}) or 0.13 mW m^{-2}/ppbv. The magnitude of this feedback is primarily controlled by changes in methane and stratospheric water vapor with smaller contribution from increasing tropospheric ozone. The importance of CH_4 highlights the benefits of controlling CH_4 emissions to minimize the radiative forcing associated with increasing H_2 usage.

Table 1: Global tropospheric budget of H_2 [a]

	This work	Other estimates[b]
Source		
Emission	32.3 [29.9–37.1]	28–48
Anthropogenic	14.3 [13.4–15.8]	11–25
Biomass burning	9 [7.3–12.6]	8–20
Nitrogen fixation	9	
Soil	3	1–11
Ocean	6	3–6
Chemical production	42.1 [40.7–43.3]	30–41[b], 64–77[c]
Tropospheric loss		
Dry deposition	54.7 [53.5–56.3]	55–60[b], 85–88[c]
Chemical loss	20.4 [19.5–20.9]	15–19
Tropospheric burden [Tg H_2]	157.4 [154.5–162.3]	136–157
Tropospheric lifetime [years]	2.1	1.9–2.3[b], 1.4[c]

[a] Tg/yr over the 1995–2014 average. The range is indicated in bracket. [b] from bottom-up estimates [27, 100, 71, 101, 69, 102, 28, 70, 103, 104, 56]. [c] from top-down estimates [101, 102]

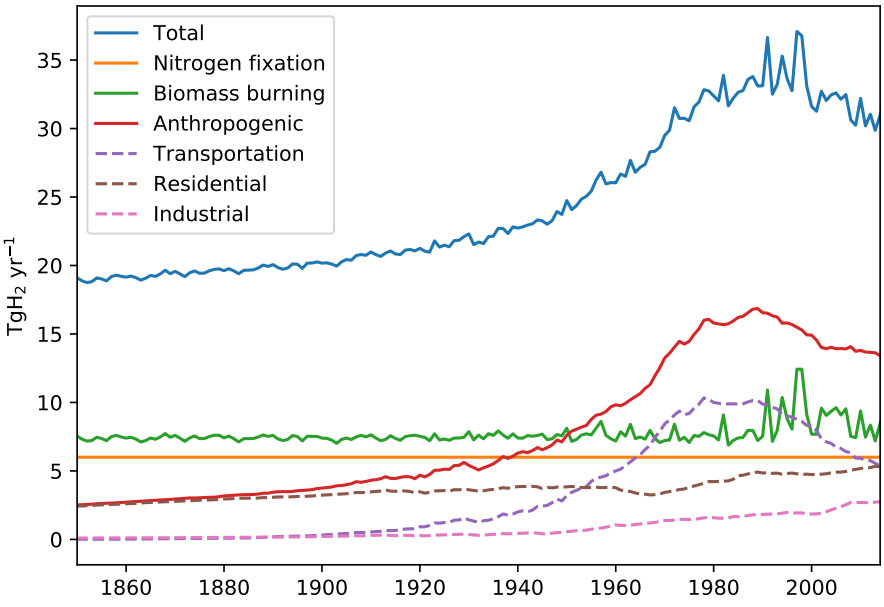

Figure 1: Historical H_2 emission

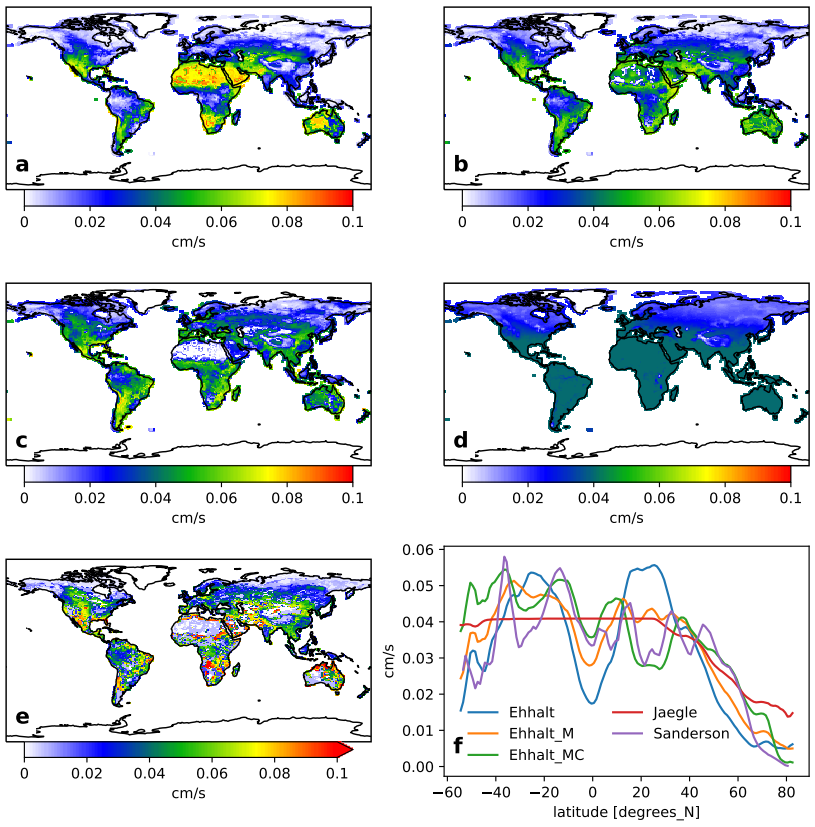

Figure 2: Simulated annual H_2 deposition velocity averaged over the 1989-2014 period based on (a) Ehhalt and Rohrer [66] (equation 2), (b) Ehhalt and Rohrer [66] with global soil moisture adjustment (Ehhalt_M), (c) Ehhalt and Rohrer [66] with global soil moisture and organic soil C adjustment (Ehhalt_MC), (d) Sanderson et al. [71], (e) Price et al. [69]. Panel (f) shows the meridional distribution of H_2 deposition velocity.

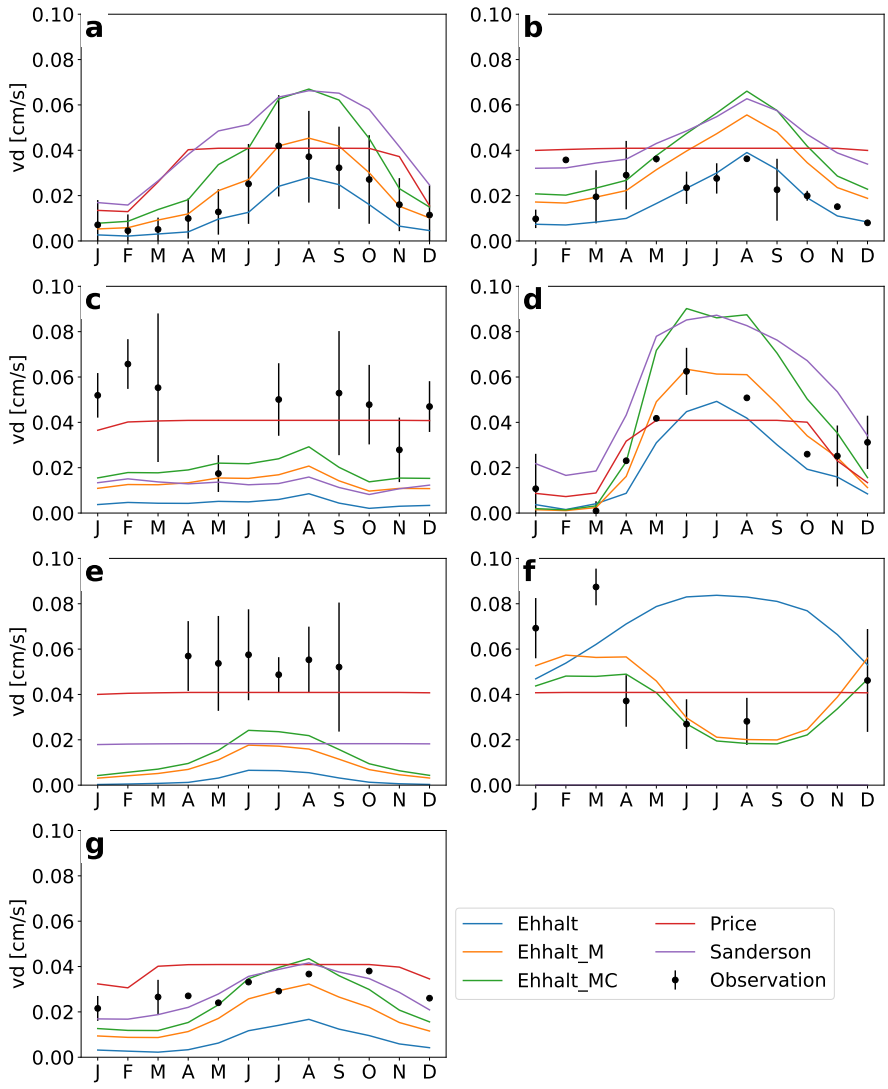

Figure 3: Comparison between simulated and observed H_2 deposition velocity at (a) Harvard Forest (temperate forest [36]), (b) Gif-sur-Yvette (pasture [105], (c) Tsukuba (agricultural land [31]. (d) Helsinki (forest, [106]), (e) Mace Head (peat, [107]) (f) San Jacinto Mountain Reserve (desert, [33]), (g) Heidelberg (semi-urban, [108])

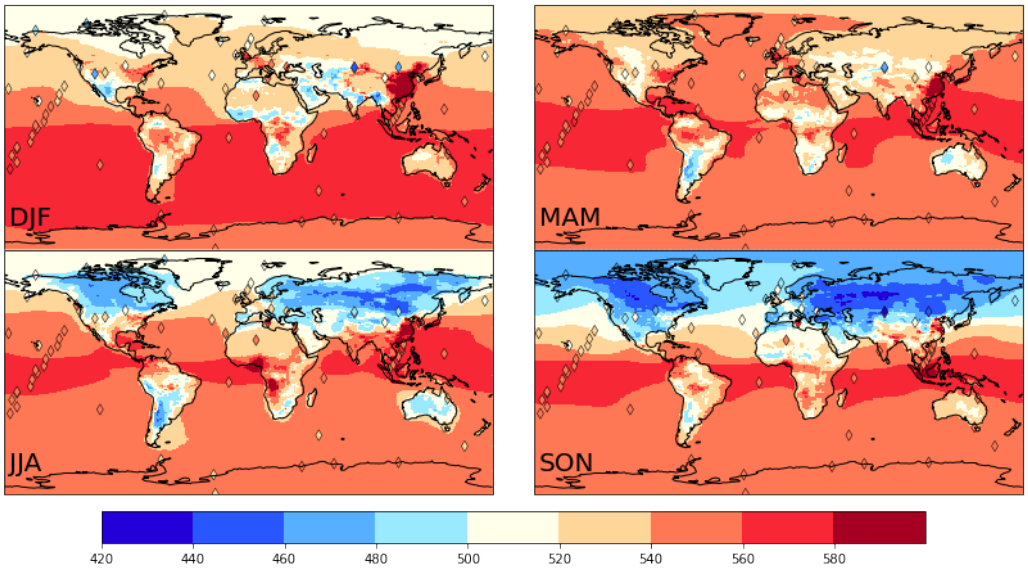

Figure 4: Seasonal maps of modeled surface H_2 dry mixing ratios (ppbv) averaged over the 1995-2005 period using the Ehhalt_MC parameterization. Observations from NOAA, CSIRO, and AGAGE are shown as colored diamonds. Both models and observations are averaged over the 1995–2005 period.

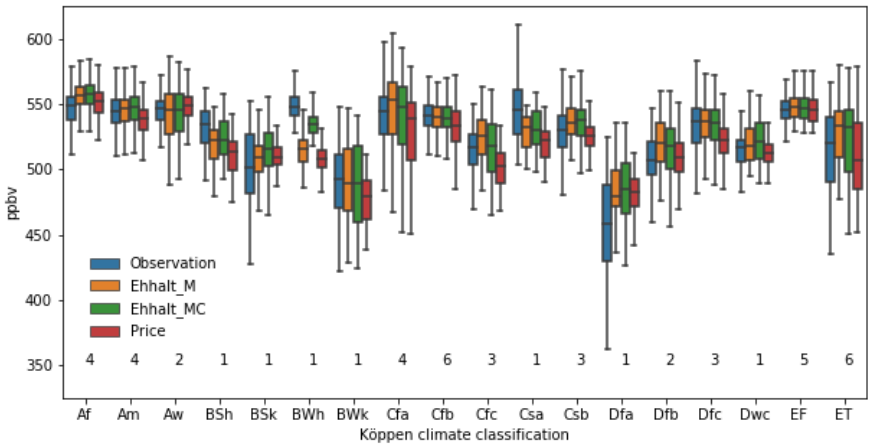

Figure 5: Observed and simulated H_2 grouped by climate zone over the 1992-2014 period. The box shows the quartiles of the dataset while the whiskers extend to show the rest of the distribution. Outliers are indicated by dots. The numbers of sites contributing to each climate zone is indicated. climate zone Af: Tropical rainforest climate, Am: Tropical monsoon climate, Aw: Tropical savanna climate with dry-winter characteristics, BSk: Cold semi-arid climate, BSh: Hot semi-arid climate, BWh: Hot desert climate, BWk: Cold desert climate, Csa: Mediterranean hot summer climates, Csb: Warm-summer Mediterranean climate, Cfa: Humid subtropical climate, Cfb: Oceanic climate, Cfc: Subpolar oceanic climate, Dfa: Hot summer continental climates, Dfb: Warm summer continental or hemiboreal climates, Dfc: Subarctic climate, Dwc: Monsoon-influenced subarctic climate, EF: Ice cap climate, ET: Tundra climate

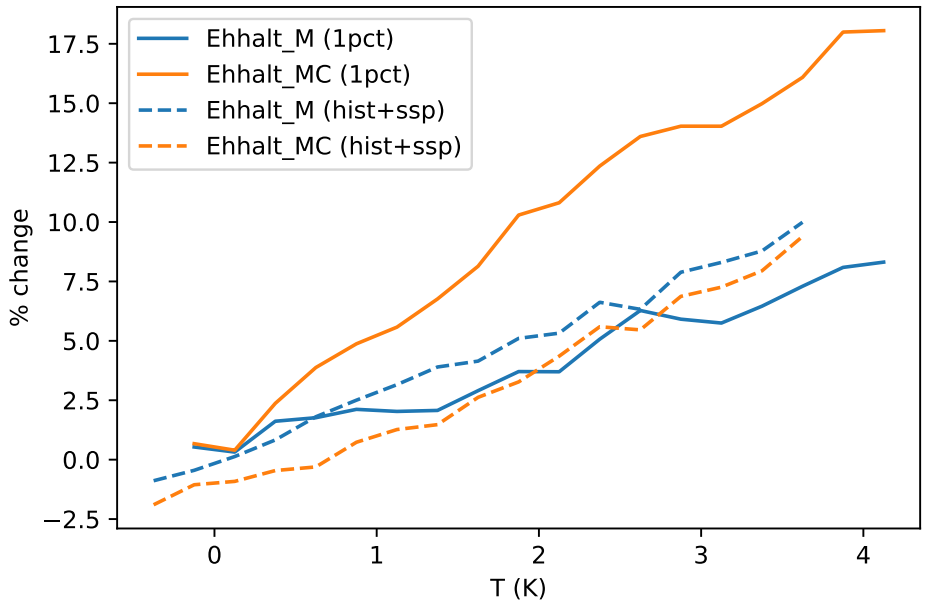

Figure 6: Simulated change in the global average H_2 deposition velocity with temperature under CO_2-forcing (solid lines) and historical and projected forcing (hist_ssp (dash line)) scenarios. The sensitivity of $v_d(H_2)$ to warming from the Ehhalt_M and Ehhalt_MC parameterizations are shown in blue and orange, respectively.

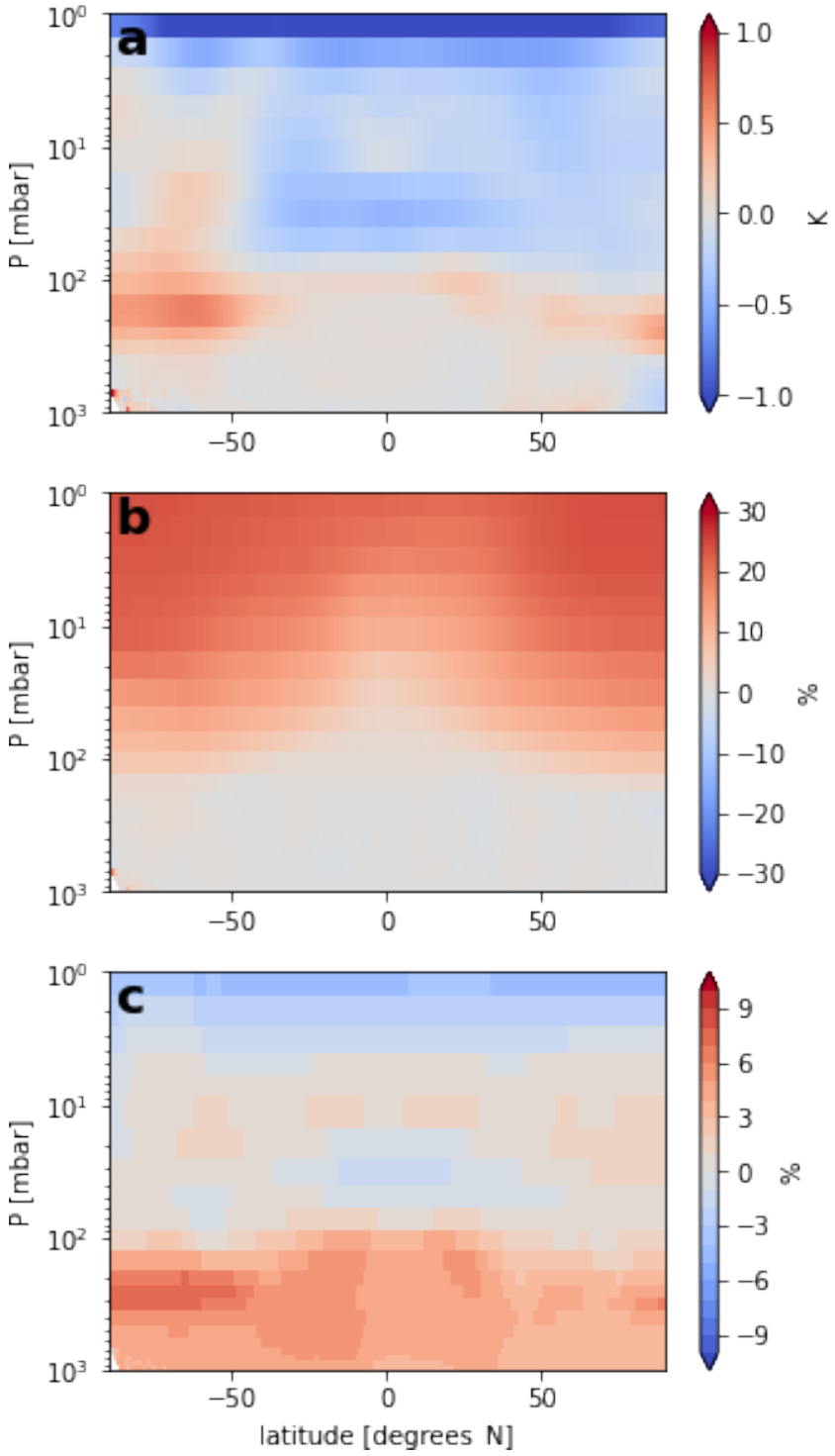

Figure 7: Simulated change in temperature (a), water vapor (b), and O_3 (c) in response to a 200 Tg/yr increase in H_2 emissions.

References

[1] Hydrogen council, Hydrogen scaling up. a sustainable pathway for the global energy transition, 2017.

[2] T. da Silva Veras, T. S. Mozer, D. da Costa Rubim Messeder dos Santos, A. da Silva César, Hydrogen: Trends, production and characterization of the main process worldwide, International Journal of Hydrogen Energy 42 (2017) 2018–2033. URL: https://doi.org/10.1016/j.ijhydene.2016.08.219. doi:10.1016/j.ijhydene.2016.08.219.

[3] I. Staffell, D. Scamman, A. V. Abad, P. Balcombe, P. E. Dodds, P. Ekins, N. Shah, K. R. Ward, The role of hydrogen and fuel cells in the global energy system, Energy & Environmental Science 12 (2019) 463–491. doi:10.1039/c8ee01157e.

[4] J. Abe, A. Popoola, E. Ajenifuja, O. Popoola, Hydrogen energy, economy and storage: Review and recommendation, International Journal of Hydrogen Energy 44 (2019) 15072–15086. URL: https://doi.org/10.1016/j.ijhydene.2019.04.068. doi:10.1016/j.ijhydene.2019.04.068.

[5] F. Dawood, M. Anda, G. Shafiullah, Hydrogen production for energy: An overview, International Journal of Hydrogen Energy 45 (2020) 3847–3869. URL: http://dx.doi.org/10.1016/j.ijhydene.2019.12.059. doi:10.1016/j.ijhydene.2019.12.059.

[6] J. Holladay, J. Hu, D. King, Y. Wang, An overview of hydrogen production technologies, Catalysis Today 139 (2009) 244–260. URL: http://dx.doi.org/10.1016/j.cattod.2008.08.039. doi:10.1016/j.cattod.2008.08.039.

[7] P. Nikolaidis, A. Poullikkas, A comparative overview of hydrogen production processes, Renewable and Sustainable Energy Reviews 67 (2017) 597–611. URL: http://dx.doi.org/10.1016/j.rser.2016.09.044. doi:10.1016/j.rser.2016.09.044.

[8] B. Sørensen, G. Spazzafumo, Hydrogen, in: Hydrogen and Fuel Cells, Elsevier, 2018, pp. 5–105. doi:10.1016/b978-0-08-100708-2.00002-3.

[9] M. El-Shafie, S. Kambara, Y. Hayakawa, Hydrogen production technologies overview, Journal of Power and Energy Engineering 07 (2019) 107–154. URL: http://dx.doi.org/10.4236/jpee.2019.71007. doi:10.4236/jpee.2019.71007.

[10] IRENA, Hydrogen: A renewable energy perspective, 2019.

[11] W. Leighty, Running the world on renewables: Hydrogen transmission pipelines and firming geologic storage, International Journal of Energy Research 32 (2008) 408–426. doi:10.1002/er.1373.

[12] M. A. Pellow, C. J. M. Emmott, C. J. Barnhart, S. M. Benson, Hydrogen or batteries for grid storage? a net energy analysis, Energy & Environmental Science 8 (2015) 1938–1952. doi:10.1039/c4ee04041d.

[13] S. Schiebahn, T. Grube, M. Robinius, V. Tietze, B. Kumar, D. Stolten, Power to gas: Technological overview, systems analysis and economic assessment for a case study in Germany, International Journal of Hydrogen Energy 40 (2015) 4285–4294. doi:10.1016/j.ijhydene.2015.01.123.

[14] D. G. Caglayan, N. Weber, H. U. Heinrichs, J. Linßen, M. Robinius, P. A. Kukla, D. Stolten, Technical potential of salt caverns for hydrogen storage in Europe, International Journal of Hydrogen Energy 45 (2020) 6793–6805. doi:10.1016/j.ijhydene.2019.12.161.

[15] R. P. by the IEA for the G20, The Future of Hydrogen – Seizing today's opportunities, Technical Report, International Energy Agency, Paris, France, 2019.

[16] K. Damen, M. v. Troost, A. Faaij, W. Turkenburg, A comparison of electricity and hydrogen production systems with CO_2 capture and storage. part a: Review and selection of promising conversion and capture technologies, Progress in Energy and Combustion Science 32 (2006) 215–246. URL: http://dx.doi.org/10.1016/j.pecs.2005.11.005. doi:10.1016/j.pecs.2005.11.005.

[17] M. G. Schultz, Air pollution and climate-forcing impacts of a global hydrogen economy, Science 302 (2003) 624–627. URL: https://doi.org/10.1126/science.1089527. doi:10.1126/science.1089527.

[18] M. Z. Jacobson, Effects of wind-powered hydrogen fuel cell vehicles on stratospheric ozone and global climate, Geophysical Research Letters 35 (2008). URL: https://doi.org/10.1029/2008gl035102. doi:10.1029/2008gl035102.

[19] B. van Ruijven, J.-F. Lamarque, D. P. van Vuuren, T. Kram, H. Eerens, Emission scenarios for a global hydrogen economy and the consequences for global air pollution, Global Environmental Change 21 (2011) 983–994. URL: http://dx.doi.org/10.1016/j.gloenvcha.2011.03.013. doi:10.1016/j.gloenvcha.2011.03.013.

[20] D. Wang, W. Jia, S. C. Olsen, D. J. Wuebbles, M. K. Dubey, A. A. Rockett, Impact of a future H_2-based road transportation sector on the composition and chemistry of the atmosphere – part 1: Tropospheric composition and air quality, Atmospheric Chemistry and Physics 13 (2013) 6117–6137. URL: https://doi.org/10.5194/acp-13-6117-2013. doi:10.5194/acp-13-6117-2013.

[21] R. G. Derwent, W. J. Collins, C. E. Johnson, D. S. Stevenson, Transient behaviour of tropospheric ozone precursors in a global 3-d ctm and their indirect greenhouse effects, Climatic Change 49 (2001) 463–487. URL: https://doi.org/10.1023/a:1010648913655. doi:10.1023/a:1010648913655.

[22] R. Derwent, P. Simmonds, S. O'Doherty, A. Manning, W. Collins, D. Stevenson, Global environmental impacts of the hydrogen economy, International Journal of Nuclear Hydrogen Production and Applications 1 (2006) 57. URL: https://doi.org/10.1504/ijnhpa.2006.009869. doi:10.1504/ijnhpa.2006.009869.

[23] R. G. Derwent, D. S. Stevenson, S. R. Utembe, M. E. Jenkin, A. H. Khan, D. E. Shallcross, Global modelling

studies of hydrogen and its isotopomers using STOCHEM-CRI: Likely radiative forcing consequences of a future hydrogen economy, International Journal of Hydrogen Energy 45 (2020) 9211–9221. URL: https://doi.org/10.1016/j.ijhydene.2020.01.125. doi:10.1016/j.ijhydene.2020.01.125.

[24] T. K. Tromp, Potential environmental impact of a hydrogen economy on the stratosphere, Science 300 (2003) 1740–1742. URL: https://doi.org/10.1126/science.1085169. doi:10.1126/science.1085169.

[25] B. Vogel, T. Feck, J.-U. Grooß, M. Riese, Impact of a possible future global hydrogen economy on arctic stratospheric ozone loss, Energy & Environmental Science 5 (2012) 6445. URL: https://doi.org/10.1039/c2ee03181g. doi:10.1039/c2ee03181g.

[26] D. Wang, W. Jia, S. C. Olsen, D. J. Wuebbles, M. K. Dubey, A. A. Rockett, Impact of a future H_2-based road transportation sector on the composition and chemistry of the atmosphere – part 2: Stratospheric ozone, Atmospheric Chemistry and Physics 13 (2013) 6139–6150. URL: https://doi.org/10.5194/acp-13-6139-2013. doi:10.5194/acp-13-6139-2013.

[27] P. C. Novelli, P. M. Lang, K. A. Masarie, D. F. Hurst, R. Myers, J. W. Elkins, Molecular hydrogen in the troposphere: Global distribution and budget, Journal of Geophysical Research: Atmospheres 104 (1999) 30427–30444. URL: https://doi.org/10.1029/1999jd900788. doi:10.1029/1999jd900788.

[28] D. H. Ehhalt, F. Rohrer, The tropospheric cycle of H_2: a critical review, Tellus B: Chemical and Physical Meteorology 61 (2009) 500–535. URL: https://doi.org/10.1111/j.1600-0889.2009.00416.x. doi:10.1111/j.1600-0889.2009.00416.x.

[29] R. Conrad, W. Seiler, Influence of temperature, moisture, and organic carbon on the flux of H_2 and CO between soil and atmosphere: Field studies in subtropical regions, Journal of Geophysical Research 90 (1985) 5699. URL: https://doi.org/10.1029/jd090id03p05699. doi:10.1029/jd090id03p05699.

[30] S. Yonemura, S. Kawashima, H. Tsuruta, Continuous measurements of CO and H_2 deposition velocities onto an andisol: uptake control by soil moisture, Tellus B: Chemical and Physical Meteorology 51 (1999) 688–700. URL: https://doi.org/10.3402/tellusb.v51i3.16465. doi:10.3402/tellusb.v51i3.16465.

[31] S. Yonemura, M. Yokozawa, S. Kawashima, H. Tsuruta, Model analysis of the influence of gas diffusivity in soil on CO and H_2 uptake, Tellus B: Chemical and Physical Meteorology 52 (2000) 919–933. URL: https://doi.org/10.3402/tellusb.v52i3.17075. doi:10.3402/tellusb.v52i3.17075.

[32] N. V. Smith-Downey, J. T. Randerson, J. M. Eiler, Temperature and moisture dependence of soil H_2 uptake measured in the laboratory, Geophysical Research Letters 33 (2006). URL: https://doi.org/10.1029/2006gl026749. doi:10.1029/2006gl026749.

[33] N. V. Smith-Downey, J. T. Randerson, J. M. Eiler, Molecular hydrogen uptake by soils in forest, desert, and marsh ecosystems in California, Journal of Geophysical Research 113 (2008). URL: https://doi.org/10.1029/2008jg000701. doi:10.1029/2008jg000701.

[34] S. Schmitt, A. Hanselmann, U. Wollschläger, S. Hammer, I. Levin., Investigation of parameters controlling the soil sink of atmospheric molecular hydrogen, Tellus B: Chemical and Physical Meteorology 61 (2009) 416–423. URL: https://doi.org/10.1111/j.1600-0889.2008.00402.x. doi:10.1111/j.1600-0889.2008.00402.x.

[35] D. H. Ehhalt, F. Rohrer, The dependence of soil H_2 uptake on temperature and moisture: a reanalysis of laboratory data, Tellus B: Chemical and Physical Meteorology 63 (2011) 1040–1051. URL: https://doi.org/10.1111/j.1600-0889.2011.00581.x. doi:10.1111/j.1600-0889.2011.00581.x.

[36] L. K. Meredith, R. Commane, T. F. Keenan, S. T. Klosterman, J. W. Munger, P. H. Templer, J. Tang, S. C. Wofsy, R. G. Prinn, Ecosystem

fluxes of hydrogen in a mid-latitude forest driven by soil microorganisms and plants, Global Change Biology 23 (2016) 906–919. URL: https://doi.org/10.1111/gcb.13463. doi:10.1111/gcb.13463.

[37] P. Constant, L. Poissant, R. Villemur, Isolation of streptomyces sp. PCB7, the first microorganism demonstrating high-affinity uptake of tropospheric H_2, The ISME Journal 2 (2008) 1066–1076. URL: https://doi.org/10.1038/ismej.2008.59. doi:10.1038/ismej.2008.59.

[38] P. Constant, S. P. Chowdhury, L. Hesse, R. Conrad, Co-localization of atmospheric H_2 oxidation activity and high affinity H_2-oxidizing bacteria in non-axenic soil and sterile soil amended with streptomyces sp. PCB7, Soil Biology and Biochemistry 43 (2011) 1888–1893. URL: https://doi.org/10.1016/j.soilbio.2011.05.009. doi:10.1016/j.soilbio.2011.05.009.

[39] A. Myagkiy, F. Brunet, C. Popov, R. Krüger, H. Guimarães, R. S. Sousa, L. Charlet, I. Moretti, H_2 dynamics in the soil of a H_2-emitting zone (São Francisco Basin, Brazil): Microbial uptake quantification and reactive transport modelling, Applied Geochemistry 112 (2020) 104474. URL: https://doi.org/10.1016/j.apgeochem.2019.104474. doi:10.1016/j.apgeochem.2019.104474.

[40] S. Piché-Choquette, J. Tremblay, S. G. Tringe, P. Constant, H_2-saturation of high affinity H_2-oxidizing bacteria alters the ecological niche of soil microorganisms unevenly among taxonomic groups, PeerJ 4 (2016) e1782. URL: http://dx.doi.org/10.7717/peerj.1782. doi:10.7717/peerj.1782.

[41] C. Greening, M. Berney, K. Hards, G. M. Cook, R. Conrad, A soil actinobacterium scavenges atmospheric H_2 using two membrane-associated, oxygen-dependent [NiFe] hydrogenases, Proceedings of the National Academy of Sciences 111 (2014) 4257–4261. URL: https://doi.org/10.1073/pnas.1320586111. doi:10.1073/pnas.1320586111.

[42] C. Greening, S. G. Villas-Bôas, J. R. Robson, M. Berney, G. M. Cook, The growth and survival of mycobacterium smegmatis is enhanced by co-metabolism of atmospheric H_2, PLoS ONE 9 (2014) e103034.

URL: http://dx.doi.org/10.1371/journal.pone.0103034. doi:10.1371/journal.pone.0103034.

[43] C. Greening, A. Biswas, C. R. Carere, C. J. Jackson, M. C. Taylor, M. B. Stott, G. M. Cook, S. E. Morales, Genomic and metagenomic surveys of hydrogenase distribution indicate H_2 is a widely utilised energy source for microbial growth and survival, The ISME Journal 10 (2015) 761–777. URL: https://doi.org/10.1038/ismej.2015.153. doi:10.1038/ismej.2015.153.

[44] M. Ji, C. Greening, I. Vanwonterghem, C. R. Carere, S. K. Bay, J. A. Steen, K. Montgomery, T. Lines, J. Beardall, J. van Dorst, I. Snape, M. B. Stott, P. Hugenholtz, B. C. Ferrari, Atmospheric trace gases support primary production in Antarctic desert surface soil, Nature 552 (2017) 400–403. URL: https://doi.org/10.1038/nature25014. doi:10.1038/nature25014.

[45] Z. Yang, Y. Zhang, Y. Lv, W. Yan, X. Xiao, B. Sun, H. Ma, H_2 metabolism revealed by metagenomic analysis of subglacial sediment from East Antarctica, Journal of Microbiology 57 (2019) 1095–1104. URL: http://dx.doi.org/10.1007/s12275-019-9366-2. doi:10.1007/s12275-019-9366-2.

[46] S. Bay, B. Ferrari, C. Greening, Life without water: how do bacteria generate biomass in desert ecosystems?, Microbiology Australia 39 (2018) 28. URL: http://dx.doi.org/10.1071/MA18008. doi:10.1071/ma18008.

[47] C. Greening, P. Constant, K. Hards, S. E. Morales, J. G. Oakeshott, R. J. Russell, M. C. Taylor, M. Berney, R. Conrad, G. M. Cook, Atmospheric hydrogen scavenging: from enzymes to ecosystems, Applied and Environmental Microbiology 81 (2014) 1190–1199. URL: https://doi.org/10.1128/aem.03364-14. doi:10.1128/aem.03364-14.

[48] C. Greening, C. R. Carere, R. Rushton-Green, L. K. Harold, K. Hards, M. C. Taylor, S. E. Morales, M. B. Stott, G. M. Cook, Persistence of the dominant soil phylum acidobacteria by trace gas scavenging, Proceedings of the National Academy of Sciences 112 (2015)

10497–10502. URL: https://doi.org/10.1073/pnas.1508385112. doi:10.1073/pnas.1508385112.

[49] M. Khdhiri, L. Hesse, M. E. Popa, L. Quiza, I. Lalonde, L. K. Meredith, T. Röckmann, P. Constant, Soil carbon content and relative abundance of high affinity H_2-oxidizing bacteria predict atmospheric H_2 soil uptake activity better than soil microbial community composition, Soil Biology and Biochemistry 85 (2015) 1–9. URL: https://doi.org/10.1016/j.soilbio.2015.02.030. doi:10.1016/j.soilbio.2015.02.030.

[50] M. Zhao, J.-C. Golaz, I. M. Held, H. Guo, V. Balaji, R. Benson, J.-H. Chen, X. Chen, L. J. Donner, J. P. Dunne, K. Dunne, J. Durachta, S.-M. Fan, S. M. Freidenreich, S. T. Garner, P. Ginoux, L. M. Harris, L. W. Horowitz, J. P. Krasting, A. R. Langenhorst, Z. Liang, P. Lin, S.-J. Lin, S. L. Malyshev, E. Mason, P. C. D. Milly, Y. Ming, V. Naik, F. Paulot, D. Paynter, P. Phillipps, A. Radhakrishnan, V. Ramaswamy, T. Robinson, D. Schwarzkopf, C. J. Seman, E. Shevliakova, Z. Shen, H. Shin, L. G. Silvers, J. R. Wilson, M. Winton, A. T. Wittenberg, B. Wyman, B. Xiang, The GFDL global atmosphere and land model AM4.0/LM4.0 - 1. simulation characteristics with prescribed SSTs, J. Adv. Model. Earth Syst. (2018). URL: https://doi.org/10.1002/2017ms001208. doi:10.1002/2017ms001208.

[51] J. P. Dunne, L. W. Horowitz, A. J. Adcroft, P. Ginoux, I. M. Held, J. G. John, J. P. Krasting, S. Malyshev, V. Naik, F. Paulot, E. Shevliakova, C. A. Stock, N. Zadeh, V. Balaji, C. Blanton, K. A. Dunne, C. Dupuis, J. Durachta, R. Dussin, P. P. G. Gauthier, S. M. Griffies, H. Guo, R. W. Hallberg, M. Harrison, J. He, W. Hurlin, C. McHugh, R. Menzel, P. C. D. Milly, S. Nikonov, D. J. Paynter, J. Ploshay, A. Radhakrishnan, K. Rand, B. G. Reichl, T. Robinson, D. M. Schwarzkopf, L. T. Sentman, S. Underwood, H. Vahlenkamp, M. Winton, A. T. Wittenberg, B. Wyman, Y. Zeng, M. Zhao, The GFDL earth system model version 4.1 (GFDL-ESM 4.1): Overall coupled model description and simulation characteristics, Journal of Advances in Modeling Earth Systems (2020). doi:10.1029/2019ms002015.

[52] L. W. Horowitz, V. Naik, F. Paulot, P. A. Ginoux, J. P. Dunne, J. Mao,

J. Schnell, X. Chen, J. He, J. G. John, M. Lin, P. Lin, S. Malyshev, D. Paynter, E. Shevliakova, M. Zhao, The GFDL global atmospheric chemistry-climate model AM4.1: Model description and simulation characteristics, Journal of Advances in Modeling Earth Systems (2020). doi:10.1029/2019ms002032.

[53] K. E. Taylor, D. Williamson, F. Zwiers, The sea surface temperature and sea-ice concentration boundary conditions for AMIP II simulations, Program for Climate Model Diagnosis and Intercomparison, Lawrence Livermore National Laboratory, University of California, 2000.

[54] N. A. Rayner, D. E. Parker, E. B. Horton, C. K. Folland, L. V. Alexander, D. P. Rowell, E. C. Kent, A. Kaplan, Global analyses of sea surface temperature, sea ice, and night marine air temperature since the late nineteenth century, J. Geophys. Res. Atmos. 108 (2003) 4407. URL: http://dx.doi.org/10.1029/2002JD002670. doi:10.1029/2002JD002670.

[55] M. J. E. van Marle, S. Kloster, B. I. Magi, J. R. Marlon, A.-L. Daniau, R. D. Field, A. Arneth, M. Forrest, S. Hantson, N. M. Kehrwald, W. Knorr, G. Lasslop, F. Li, S. Mangeon, C. Yue, J. W. Kaiser, G. R. van der Werf, Historic global biomass burning emissions for CMIP6 (BB4cmip) based on merging satellite observations with proxies and fire models (1750–2015), Geosci. Model Dev. 10 (2017) 3329–3357. URL: https://doi.org/10.5194/gmd-10-3329-2017. doi:10.5194/gmd-10-3329-2017.

[56] M. O. Andreae, Emission of trace gases and aerosols from biomass burning – an updated assessment, Atmospheric Chemistry and Physics 19 (2019) 8523–8546. URL: https://doi.org/10.5194/acp-19-8523-2019. doi:10.5194/acp-19-8523-2019.

[57] S. K. Akagi, J. S. Craven, J. W. Taylor, G. R. McMeeking, R. J. Yokelson, I. R. Burling, S. P. Urbanski, C. E. Wold, J. H. Seinfeld, H. Coe, M. J. Alvarado, D. R. Weise, Evolution of trace gases and particles emitted by a chaparral fire in California, Atmos. Chem. Phys. 12 (2012) 1397–1421. URL: http://www.atmos-chem-phys.net/12/1397/2012/. doi:10.5194/acp-12-1397-2012.

[58] R. M. Hoesly, S. J. Smith, L. Feng, Z. Klimont, G. Janssens-Maenhout, T. Pitkanen, J. J. Seibert, L. Vu, R. J. Andres, R. M. Bolt, T. C. Bond, L. Dawidowski, N. Kholod, J.-I. Kurokawa, M. Li, L. Liu, Z. Lu, M. C. P. Moura, . P. R. O'Rourke, Q. Zhang, Historical (1750–2014) anthropogenic emissions of reactive gases and aerosols from the community emissions data system (CEDS), Geosci. Model Dev. 11 (2018) 369–408. URL: https://www.geosci-model-dev.net/11/369/2018/. doi:10.5194/gmd-11-369-2018.

[59] M. K. Vollmer, S. Walter, J. Mohn, M. Steinbacher, S. W. Bond, T. Röckmann, S. Reimann, Molecular hydrogen (H_2) combustion emissions and their isotope (D/H) signatures from domestic heaters, diesel vehicle engines, waste incinerator plants, and biomass burning, Atmospheric Chemistry and Physics 12 (2012) 6275–6289. URL: https://doi.org/10.5194/acp-12-6275-2012. doi:10.5194/acp-12-6275-2012.

[60] D. S. Newsome, The water-gas shift reaction, Catalysis Reviews 21 (1980) 275–318. URL: http://dx.doi.org/10.1080/03602458008067535. doi:10.1080/03602458008067535.

[61] J. Lathière, D. A. Hauglustaine, A. D. Friend, N. De Noblet-Ducoudré, N. Viovy, G. A. Folberth, Impact of climate variability and land use changes on global biogenic volatile organic compound emissions, Atmos. Chem. Phys. 6 (2006) 2129–2146.

[62] C. Granier, J. F. Lamarque, A. Mieville, J. F. Müller, J. Olivier, J. Orlando, J. Peters, G. Petron, G. Tyndall, S. Wallens, POET, a database of surface emissions of ozone precursors, available on internet at http://www.aero.jussieu.fr/projet/ACCENT/POET.php, Technical Report, 2005.

[63] A. B. Guenther, X. Jiang, C. L. Heald, T. Sakulyanontvittaya, T. Duhl, L. K. Emmons, X. Wang, The model of emissions of gases and aerosols from nature version 2.1 (MEGAN2.1): an extended and updated framework for modeling biogenic emissions, Geoscientific Model Development 5 (2012) 1471–1492. doi:10.5194/gmd-5-1471-2012.

[64] O. Wild, X. Zhu, M. J. Prather, Fast-J: Accurate simulation of in- and below-cloud photolysis in tropospheric chemical models, Journal of Atmospheric Chemistry 37 (2000) 245–282. URL: https://doi.org/10.1023/a:1006415919030. doi:10.1023/a:1006415919030.

[65] S. Sander, R. Friedl, J. Barker, D. Golden, M. Kurylo, P. Wine, J. Abbatt, J. Burkholder, C. Kolb, G. Moortgat, R. Huie, V. Orkin, Chemical Kinetics and Photochemical Data for Use in Atmospheric Studies Evaluation Number 17, National Aeronautics and Space Administration, Jet Propulsion Laboratory, California Institute of Technology, 2011.

[66] D. Ehhalt, F. Rohrer, Deposition velocity of H_2: a new algorithm for its dependence on soil moisture and temperature, Tellus B: Chemical and Physical Meteorology 65 (2013) 19904. URL: https://doi.org/10.3402/tellusb.v65i0.19904. doi:10.3402/tellusb.v65i0.19904.

[67] R. J. Millington, J. P. Quirk, Permeability of porous media, Nature 183 (1959) 387–388. URL: https://doi.org/10.1038/183387a0. doi:10.1038/183387a0.

[68] B. R. Pinzer, M. Kerbrat, T. Huthwelker, H. W. Gäggeler, M. Schneebeli, M. Ammann, Diffusion of NO_x and HONO in snow: A laboratory study, Journal of Geophysical Research 115 (2010). URL: https://doi.org/10.1029/2009jd012459. doi:10.1029/2009jd012459.

[69] H. Price, L. Jaeglé, A. Rice, P. Quay, P. C. Novelli, R. Gammon, Global budget of molecular hydrogen and its deuterium content: Constraints from ground station, cruise, and aircraft observations, Journal of Geophysical Research 112 (2007). URL: https://doi.org/10.1029/2006jd008152. doi:10.1029/2006jd008152.

[70] H. Yashiro, K. Sudo, S. Yonemura, M. Takigawa, The impact of soil uptake on the global distribution of molecular hydrogen: chemical transport model simulation, Atmospheric Chemistry and Physics 11 (2011) 6701–6719. URL:

https://doi.org/10.5194/acp-11-6701-2011. doi:10.5194/acp-11-6701-2011.

[71] M. G. Sanderson, W. J. Collins, R. G. Derwent, C. E. Johnson, Simulation of global hydrogen levels using a Lagrangian three-dimensional model, Journal of Atmospheric Chemistry 46 (2003) 15–28. URL: https://doi.org/10.1023/a:1024824223232. doi:10.1023/a:1024824223232.

[72] W. Sun, K. Maseyk, C. Lett, U. Seibt, A soil diffusion–reaction model for surface cos flux: Cossm v1, Geoscientific Model Development 8 (2015) 3055–3070. URL: http://dx.doi.org/10.5194/gmd-8-3055-2015. doi:10.5194/gmd-8-3055-2015.

[73] L. Liu, Q. Zhuang, Q. Zhu, S. Liu, H. van Asperen, M. Pihlatie, Global soil consumption of atmospheric carbon monoxide: an analysis using a process-based biogeochemistry model, Atmospheric Chemistry and Physics 18 (2018) 7913–7931. URL: http://dx.doi.org/10.5194/acp-18-7913-2018. doi:10.5194/acp-18-7913-2018.

[74] X. Morel, B. Decharme, C. Delire, G. Krinner, M. Lund, B. U. Hansen, M. Mastepanov, A new process-based soil methane scheme: Evaluation over arctic field sites with the isba land surface model, Journal of Advances in Modeling Earth Systems 11 (2019) 293–326. URL: http://dx.doi.org/10.1029/2018MS001329. doi:10.1029/2018ms001329.

[75] C. Morfopoulos, P. N. Foster, P. Friedlingstein, P. Bousquet, I. C. Prentice, A global model for the uptake of atmospheric hydrogen by soils, Global Biogeochemical Cycles 26 (2012). URL: https://doi.org/10.1029/2011gb004248. doi:10.1029/2011gb004248.

[76] N. V. Smith Downey, Soil uptake of molecular hydrogen and remote sensing of soil freeze and thaw, 2006. URL: https://resolver.caltech.edu/CaltechETD:etd-08182006-105638. doi:10.7907/BXV8-HH61.

[77] P. Constant, S. P. Chowdhury, L. Hesse, J. Pratscher, R. Conrad, Genome data mining and soil survey for the novel group 5 [nife]-hydrogenase to explore the diversity and ecological importance of presumptive high-affinity H_2-oxidizing bacteria, Applied and Environmental Microbiology 77 (2011) 6027–6035. URL: http://dx.doi.org/10.1128/AEM.00673-11. doi:10.1128/aem.00673-11.

[78] L. K. Meredith, D. Rao, T. Bosak, V. Klepac-Ceraj, K. R. Tada, C. M. Hansel, S. Ono, R. G. Prinn, Consumption of atmospheric hydrogen during the life cycle of soil-dwelling actinobacteria, Environmental Microbiology Reports 6 (2013) 226–238. URL: http://dx.doi.org/10.1111/1758-2229.12116. doi:10.1111/1758-2229.12116.

[79] C. Price, J. Penner, M. Prather, NO_x from lightning 1. Global distribution based on lightning physics, J. Geophys. Res. 102 (1997) 5929–5942.

[80] R. G. Prinn, R. F. Weiss, J. Arduini, T. Arnold, H. L. DeWitt, P. J. Fraser, A. L. Ganesan, J. Gasore, C. M. Harth, O. Hermansen, et al., History of chemically and radiatively important atmospheric gases from the advanced global atmospheric gases experiment (AGAGE), Earth System Science Data 10 (2018) 985–1018. URL: http://dx.doi.org/10.5194/essd-10-985-2018. doi:10.5194/essd-10-985-2018.

[81] R. J. Francey, L. P. Steele, D. A. Spencer, R. L. Langenfelds, R. M. Law, P. B. Krummel, P. J. Fraser, D. M. Etheridge, N. Derek, S. A. Coram, L. N. Cooper, C. E. Allison, L. Porter, S. Baly, The CSIRO (Australia) measurement of greenhouse gases in the global atmosphere., Baseline Atmospheric Program Australia. Melbourne: Bureau of Meteorology and CSIRO Atmospheric Research, 2003. URL: http://hdl.handle.net/102.100.100/191835?index=1.

[82] A. Jordan, B. Steinberg, Calibration of atmospheric hydrogen measurements, Atmospheric Measurement Techniques 4 (2011) 509–521. URL: http://dx.doi.org/10.5194/amt-4-509-2011. doi:10.5194/amt-4-509-2011.

[83] S. Bond, T. Gül, S. Reimann, B. Buchmann, A. Wokaun, Emissions of anthropogenic hydrogen to the atmosphere during the potential transition to an increasingly H_2-intensive economy, International Journal of Hydrogen Energy 36 (2011) 1122–1135. URL: http://dx.doi.org/10.1016/j.ijhydene.2010.10.016. doi:10.1016/j.ijhydene.2010.10.016.

[84] S. Fujimori, T. Hasegawa, T. Masui, K. Takahashi, D. S. Herran, H. Dai, Y. Hijioka, M. Kainuma, SSP3: AIM implementation of shared socioeconomic pathways, Global Environmental Change 42 (2017) 268–283. URL: https://doi.org/10.1016/j.gloenvcha.2016.06.009. doi:10.1016/j.gloenvcha.2016.06.009.

[85] B. C. O'Neill, C. Tebaldi, D. P. van Vuuren, V. Eyring, P. Friedlingstein, G. Hurtt, R. Knutti, E. Kriegler, J.-F. Lamarque, J. Lowe, G. A. Meehl, R. Moss, K. Riahi, B. M. Sanderson, The scenario model intercomparison project (ScenarioMIP) for CMIP6, Geoscientific Model Development 9 (2016) 3461–3482. doi:10.5194/gmd-9-3461-2016.

[86] Deloitte, Australian and global hydrogen demand growth scenario analysis, 2019. URL: https://www2.deloitte.com/content/dam/Deloitte/au/Documents/future-of-cities/

[87] Shell Global, Shell sky scenario, 2019. URL: https://www.shell.com/energy-and-innovation/the-energy-future/scenarios/shell

[88] J. J. West, A. M. Fiore, V. Naik, L. W. Horowitz, M. D. Schwarzkopf, D. L. Mauzerall, Ozone air quality and radiative forcing consequences of changes in ozone precursor emissions, Geophysical Research Letters 34 (2007). URL: http://dx.doi.org/10.1029/2006GL029173. doi:10.1029/2006gl029173.

[89] A. M. Fiore, F. J. Dentener, O. Wild, C. Cuvelier, M. G. Schultz, P. Hess, C. Textor, M. Schulz, R. M. Doherty, L. W. Horowitz, et al., Multimodel estimates of intercontinental source-receptor relationships for ozone pollution, Journal of Geophysical Research 114 (2009). URL: http://dx.doi.org/10.1029/2008JD010816. doi:10.1029/2008jd010816.

[90] G. D. Thornhill, W. J. Collins, R. J. Kramer, D. Olivi, F. O'Connor, N. L. Abraham, S. E. Bauer, M. Deushi, L. Emmons, P. Forster, L. Horowitz, B. Johnson, J. Keeble, J.-F. Lamarque, M. Michou, M. Mills, J. Mulcahy, G. Myhre, P. Nabat, V. Naik, N. Oshima, M. Schulz, C. Smith, T. Takemura, S. Tilmes, T. Wu, G. Zeng, J. Zhang, Effective radiative forcing from emissions of reactive gases and aerosols – a multimodel comparison, Atmos. Chem. Phys. Discuss. (2020). doi:10.5194/acp-2019-1205.

[91] N. J. Warwick, S. Bekki, E. G. Nisbet, J. A. Pyle, Impact of a hydrogen economy on the stratosphere and troposphere studied in a 2-d model, Geophysical Research Letters 31 (2004). URL: http://dx.doi.org/10.1029/2003GL019224. doi:10.1029/2003gl019224.

[92] R. Pincus, S. A. Buehler, M. Brath, C. Crevoisier, O. Jamil, F. Evans, J. Manners, R. Menzel, E. J. Mlawer, D. J. Paynter, R. Pernak, Y. Tellier, Benchmark calculations of radiative forcing by greenhouse gase, Journal of Geophysical Research-Atmospheres (2020 (submitteed)).

[93] G. Myhre, F. Stordal, I. Gausemel, C. J. Nielsen, E. Mahieu, Line-by-line calculations of thermal infrared radiation representative for global condition: CFC-12 as an example, Journal of Quantitative Spectroscopy and Radiative Transfer 97 (2006) 317–331. doi:10.1016/j.jqsrt.2005.04.015.

[94] M. Etminan, G. Myhre, E. J. Highwood, K. P. Shine, Radiative forcing of carbon dioxide, methane, and nitrous oxide: A significant revision of the methane radiative forcing, Geophysical Research Letters 43 (2016) 12,614–12,623. URL: http://dx.doi.org/10.1002/2016GL071930. doi:10.1002/2016gl071930.

[95] R. Pincus, E. J. Mlawer, J. S. Delamere, Balancing accuracy, efficiency, and flexibility in radiation calculations for dynamical models, Journal of Advances in Modeling Earth Systems 11 (2019) 3074–3089. doi:10.1029/2019ms001621.

[96] C. J. Smith, R. J. Kramer, G. Myhre, K. Alterskjær, W. Collins, A. Sima, O. Boucher, J.-L. Dufresne, P. Nabat, M. Michou, S. Yukimoto, J. Cole, D. Paynter, H. Shiogama, F. M. O'Connor, E. Robert-

son, A. Wiltshire, T. Andrews, C. Hannay, R. Miller, L. Nazarenko, A. Kirkevåg, D. Olivié, S. Fiedler, A. Lewinschal, C. Mackallah, M. Dix, R. Pincus, P. M. Forster, Effective radiative forcing and adjustments in CMIP6 models, Atmospheric Chemistry and Physics 20 (2020) 9591–9618. doi:10.5194/acp-20-9591-2020.

[97] M. D. Zelinka, T. A. Myers, D. T. McCoy, S. Po-Chedley, P. M. Caldwell, P. Ceppi, S. A. Klein, K. E. Taylor, Causes of higher climate sensitivity in CMIP6 models, Geophysical Research Letters 47 (2020). doi:10.1029/2019gl085782.

[98] M. D. Zelinka, 2021, URL: https://github.com/mzelinka/cmip56_forcing_feedback_ecs/

[99] T. B. Richardson, P. M. Forster, C. J. Smith, A. C. Maycock, T. Wood, T. Andrews, O. Boucher, G. Faluvegi, D. Fläschner, Ø. Hodnebrog, M. Kasoar, A. Kirkevåg, J.-F. Lamarque, J. Mülmenstädt, G. Myhre, D. Olivié, R. W. Portmann, B. H. Samset, D. Shawki, D. Shindell, P. Stier, T. Takemura, A. Voulgarakis, D. Watson-Parris, Efficacy of climate forcings in PDRMIP models, Journal of Geophysical Research: Atmospheres 124 (2019) 12824–12844. doi:10.1029/2019jd030581.

[100] D. A. Hauglustaine, D. H. Ehhalt, A three-dimensional model of molecular hydrogen in the troposphere, Journal of Geophysical Research: Atmospheres 107 (2002) 4330. URL: https://doi.org/10.1029/2001jd001156. doi:10.1029/2001jd001156.

[101] T. S. Rhee, C. A. M. Brenninkmeijer, T. Röckmann, The overwhelming role of soils in the global atmospheric hydrogen cycle, Atmospheric Chemistry and Physics 6 (2006) 1611–1625. URL: https://doi.org/10.5194/acp-6-1611-2006. doi:10.5194/acp-6-1611-2006.

[102] X. Xiao, R. G. Prinn, P. G. Simmonds, L. P. Steele, P. C. Novelli, J. Huang, R. L. Langenfelds, S. O'Doherty, P. B. Krummel, P. J. Fraser, L. W. Porter, R. F. Weiss, P. Salameh, R. H. J. Wang, Optimal estimation of the soil uptake rate of molecular hydrogen from the advanced global atmospheric gases experiment and other measurements, Journal of Geophysical Re-

search 112 (2007). URL: https://doi.org/10.1029/2006jd007241. doi:10.1029/2006jd007241.

[103] G. Pieterse, M. C. Krol, A. M. Batenburg, L. P. Steele, P. B. Krummel, R. L. Langenfelds, T. Röckmann, Global modelling of H_2 mixing ratios and isotopic compositions with the TM5 model, Atmospheric Chemistry and Physics 11 (2011) 7001–7026. URL: http://dx.doi.org/10.5194/acp-11-7001-2011. doi:10.5194/acp-11-7001-2011.

[104] G. Pieterse, M. C. Krol, A. M. Batenburg, C. A. M. Brenninkmeijer, M. E. Popa, S. O'Doherty, A. Grant, L. P. Steele, P. B. Krummel, R. L. Langenfelds, et al., Reassessing the variability in atmospheric H_2 using the two-way nested TM5 model, Journal of Geophysical Research: Atmospheres 118 (2013) 3764–3780. URL: http://dx.doi.org/10.1002/jgrd.50204. doi:10.1002/jgrd.50204.

[105] S. Belviso, M. Schmidt, C. Yver, M. Ramonet, V. Gros, T. Launois, Strong similarities between night-time deposition velocities of carbonyl sulphide and molecular hydrogen inferred from semi-continuous atmospheric observations in Gif-sur-Yvette, Paris region, Tellus B: Chemical and Physical Meteorology 65 (2013) 20719. URL: http://dx.doi.org/10.3402/tellusb.v65i0.20719. doi:10.3402/tellusb.v65i0.20719.

[106] M. Lallo, T. Aalto, T. Laurila, J. Hatakka, Seasonal variations in hydrogen deposition to boreal forest soil in southern Finland, Geophysical Research Letters 35 (2008). URL: http://dx.doi.org/10.1029/2007gl032357. doi:10.1029/2007gl032357.

[107] P. Simmonds, R. Derwent, A. Manning, A. Grant, S. O'doherty, T. Spain, Estimation of hydrogen deposition velocities from 1995-2008 at mace head, ireland using a simple box model and concurrent ozone depositions, Tellus B: Chemical and Physical Meteorology 63 (2011) 40–51. URL: http://dx.doi.org/10.1111/j.1600-0889.2010.00518.x. doi:10.1111/j.1600-0889.2010.00518.x.

[108] S. Hammer, I. Levin, Seasonal variation of the molecular hydrogen uptake by soils inferred from continuous atmospheric observations in heidelberg, southwest germany, Tellus B: Chemical and Physical Meteorology 61 (2009) 556–565. URL: http://dx.doi.org/10.1111/j.1600-0889.2009.00417.x. doi:10.1111/j.1600-0889.2009.00417.x.

[109] S. K. Akagi, R. J. Yokelson, C. Wiedinmyer, M. J. Alvarado, J. S. Reid, T. Karl, J. D. Crounse, P. O. Wennberg, Emission factors for open and domestic biomass burning for use in atmospheric models, Atmos. Chem. Phys. 11 (2011) 4039–4072.

Supporting materials

Table S1: H_2 emission factor for biomass burning in g/kg of dry matter

Ecosystem	EF(H_2)
Savanna	1.7[a]
Boreal	2.03[b]
Temperate	2.03[a]
Tropical forest	3.36[a]
Peatland	1.2[c]
Agricultural	2.59[a]

[a] from Akagi et al. [109]
[b] assuming the same emission factor as temperate forest
[c] from Andreae [56]

Table S2: Emission factor for anthropogenic emissions

Sector	EF(H_2)/EF(CO)
Agriculture	0.0357 [a]
Energy	0.0143 [b]
Industrial	0.0143 [b]
Transportation	0.0357 [a]
Residential	0.0217 [c]
Solvents	0.0143 [b]
Waste	0.005 [d]
International Shipping	0.0357 [a]

[a] based on [59] gasoline EF, [b] based on Ehhalt and Rohrer [28], [c] based on [56] biofuel EF, [d] based on Vollmer et al. [59] waste EF

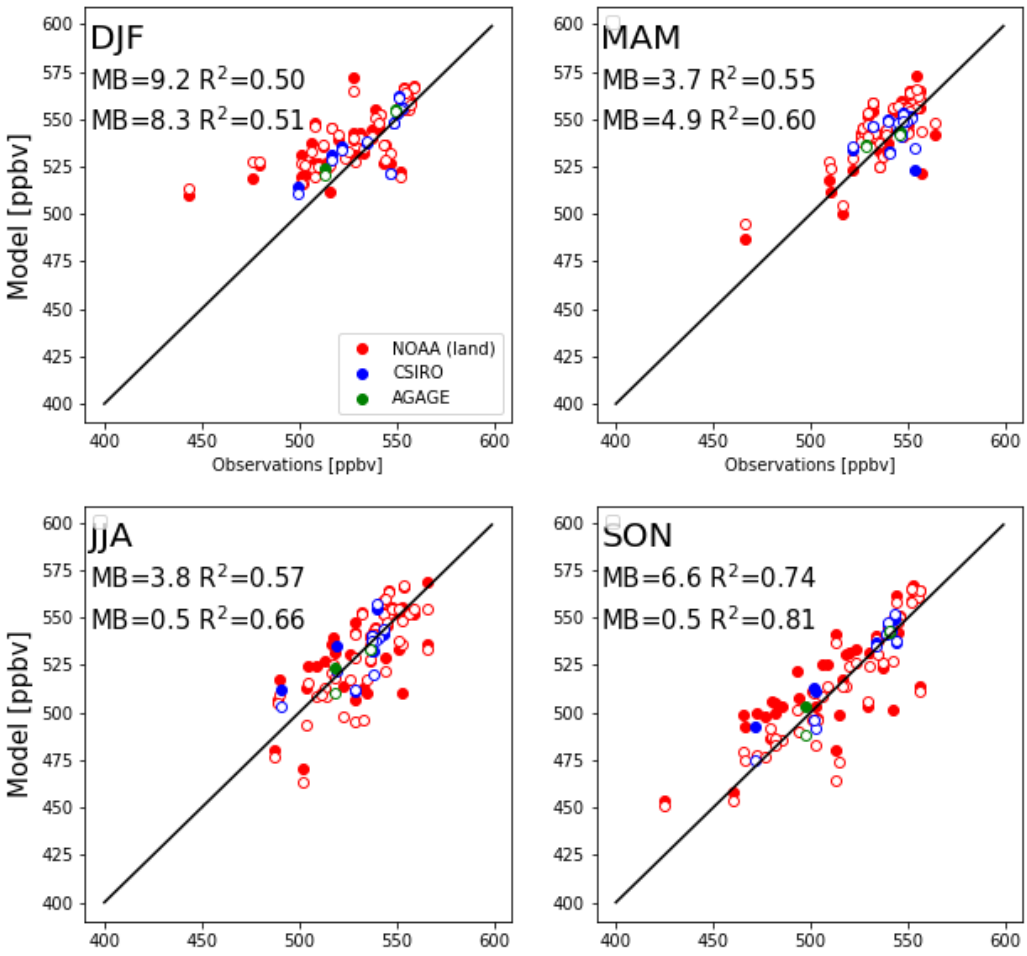

Figure S1: Comparison between seasonally averaged H_2 terrestrial observations and simulations performed with the Ehhalt_M (filled circle) and Ehhalt_MC parameterizations (open circle). Observations from CSIRO, AGAGE, and NOAA are seasonally averaged over the 1992–2014 period. Seasonal mean bias (MB) and squared correlation coefficient (R^2) are indicated for Ehhalt_M (top) and Ehhalt_MC (bottom).

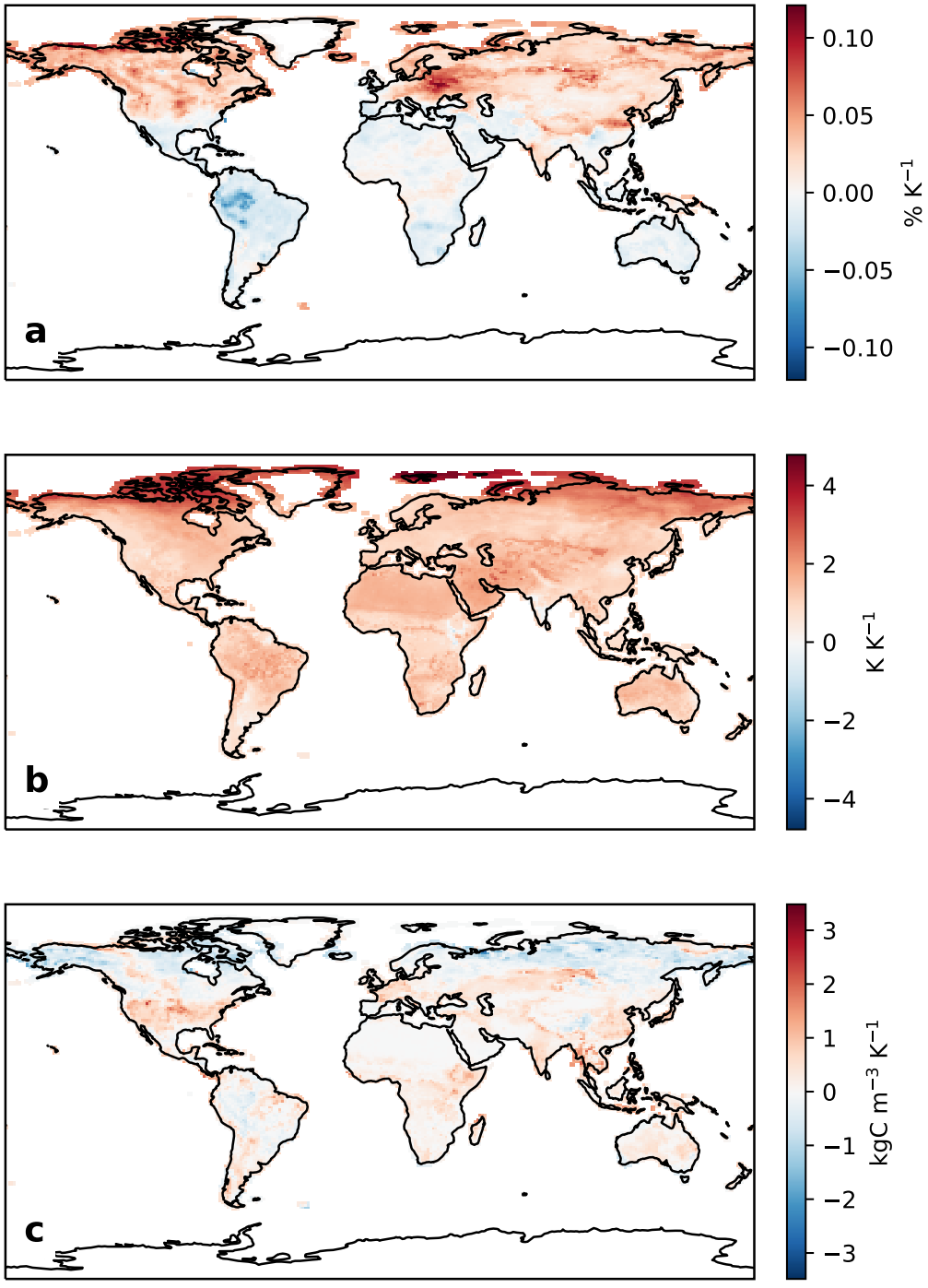

Figure S2: Simulated change in soil liquid fraction (a), temperature (b), and organic carbon content (c) normalized by the temperature change for a CO_2 doubling. Changes are averaged over the soil top 10 cm.

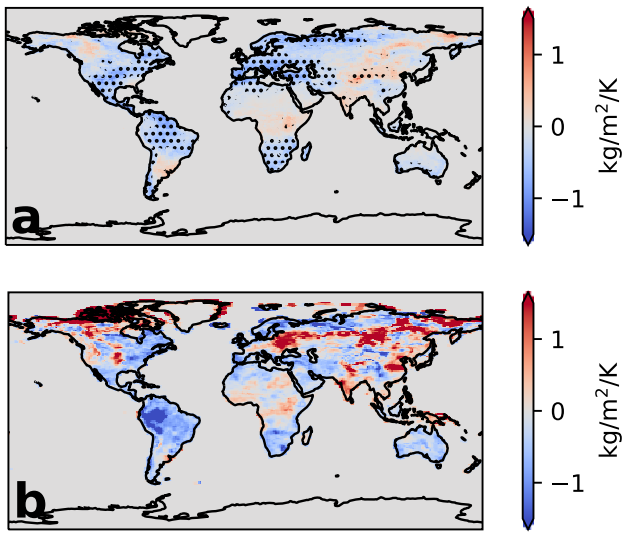

Figure S3: Same as Fig. S2 for the moisture in the upper 10 cm of the soil for the median of 22 CMIP6 models (a) and in ESM4.1 (b). Dots indicate regions where at least 17 models agree on the sign of the trends.

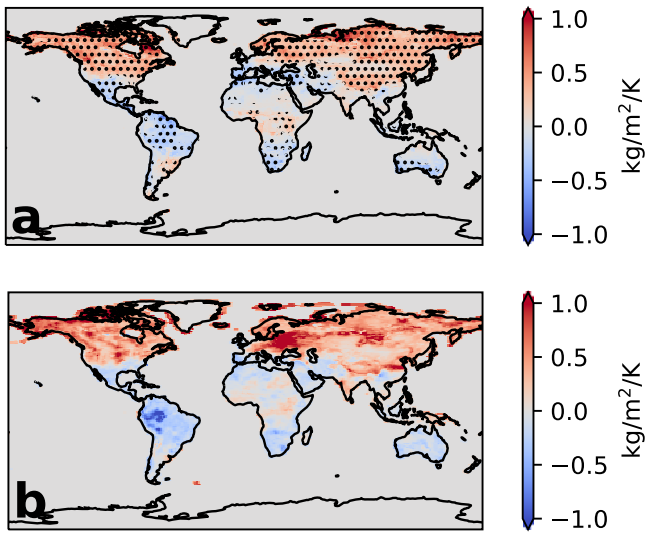

Figure S4: Same as Fig. S2 for liquid water in the upper 10 cm of the soil for the median of 9 CMIP6 models (a) and in ESM4.1 (b). Dots indicate regions where at least 7 models agree on the sign of the trends.

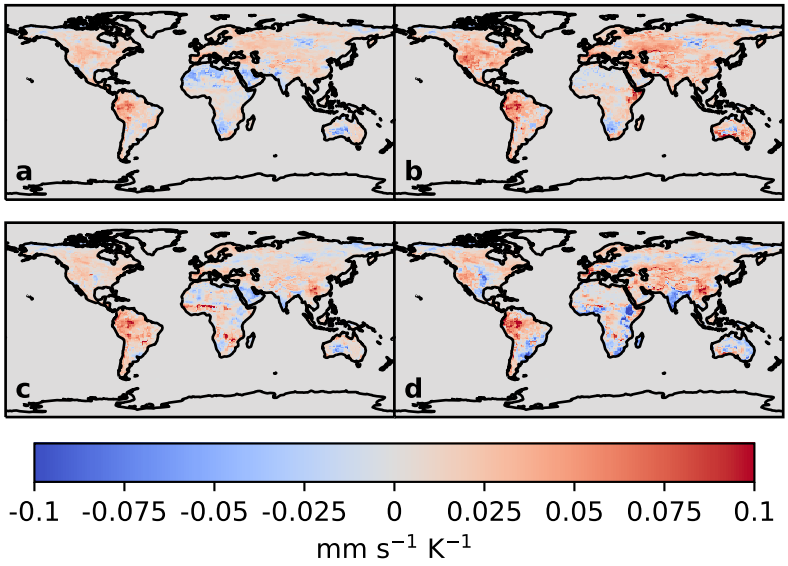

Figure S5: Change in H_2 deposition velocity associated with a 2K warming relative to preindustrial conditions. Panels (a) and (b) show the response of $v_d(H_2)$ using the Ehhalt_M and Ehhalt_MC parameterization under a 1%/yr increase of atmospheric CO_2. Panels (c) and (d) show the response of $v_d(H_2)$ using the Ehhalt_M and Ehhalt_MC parameterizations in the historical and SSP3-7.0 scenarios.